

SOLVATION OF RDX AS A FUNCTION
OF THE DIELECTRIC CONSTANT
OF THE SOLVENT

By

PAUL JOSEPH ZAHNER

Bachelor of Science

Kansas Newman College

Wichita, Kansas

1992

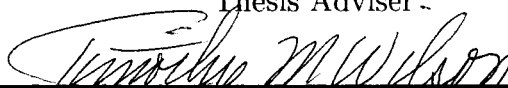
Submitted to the Faculty of the
Graduate College of the
Oklahoma State University
in partial fulfillment of
the requirements for
the Degree of
MASTER OF SCIENCE
July, 1995

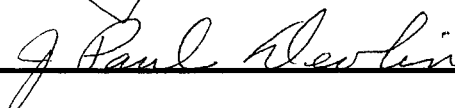
SOLVATION OF RDX AS A FUNCTION
OF THE DIELECTRIC CONSTANT
OF THE SOLVENT

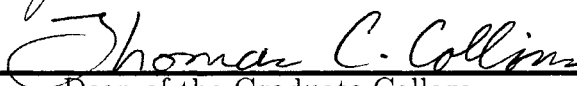
Thesis Approved:



Thesis Adviser







Dean of the Graduate College

ACKNOWLEDGEMENTS

I would like to thank all my friends and coworkers for their support, encouragement, and ideas. The following list barely scratches the surface, Candee Chambers, Ron Kay, Dan Sorescu, Yin Guo, Teressa Sutton, Bill Davis, and John Beauregard.

I would also like to thank my family, especially my parents. Although we failed to see eye to eye on many points, they were constantly behind me. The support of just being there is immeasurable. Thank You.

I need to thank Betsy Rice and Cary Chabalowski. Both of whom stayed late many a night to help analyze data, and correct the thesis. In the process they taught me more than they will ever realize.

Thanks also are extended to my advisor Dr. Thompson, for his seemingly endless patience. I know I tried him from time to time, yet he constantly helped me to focus both personally and professionally.

This work was partially supported by the Strategic Environmental Research and Development Program through the U.S. Army Research office. Thanks also to the U.S. Army Research Laboratory, Weapons Technology directorate for providing the computer resources needed to complete the calculations.

Chapter	TABLE OF CONTENTS	Page
I.	Introduction	1
II.	Theory	6
	Hartree–Fock Theory	6
	Onsager Theory	7
	Self–Consistent–Reaction Field	9
III.	Details of the Calculations	11
	Geometry Optimization and Frequency Calculations	11
	Free Energy Calculations	13
IV.	Results and Discussion	16
	Geometry	16
	Harmonic Vibrational Frequencies	18
	Infrared and Raman Intensities	18
	Atomic Charge Distributions and Dipole Moment	19
	Gibbs Free Energy of Solvation	19
V.	Conclusions	47
	BIBLIOGRAPHY	49

LIST OF TABLES

Table	Page
I. RDX Bond Lengths (\AA) vs. Dielectric Constant ϵ	31
II. RDX Bond Angles (Degrees) vs. Dielectric Constant ϵ	32
III. RDX Torsional Angles (Degrees) vs. Dielectric Constant ϵ	33
IV. Geometric Changes with respect to $\epsilon = 1$	34
V. RDX Frequencies (cm^{-1}) vs. Dielectric Constant ϵ (Part A)	35
VI. RDX Frequencies (cm^{-1}) vs. Dielectric Constant ϵ (Part B.)	36
VII. Frequency Changes (cm^{-1}) with respect to $\epsilon = 1$	37
VIII. IR Spectral Intensity (km/mol) vs. Dielectric Constant ϵ (Part A)	38
IX. IR Spectral Intensity (km/mol) vs. Dielectric Constant ϵ (Part B)	39
X. IR Spectral Intensity Changes (km/mol) with respect to $\epsilon = 1$	40
XI. Raman Spectral Intensity ($\text{\AA}^4/\text{amu}$) vs. Dielectric Con- stant ϵ (Part A)	41
XII. Raman Spectral Intensity ($\text{\AA}^4/\text{amu}$) vs. Dielectric Con- stant ϵ (Part B)	42
XIII. Raman Spectral Intensity Changes ($\text{\AA}^4/\text{amu}$) with respect to $\epsilon = 1$	43
XIV. Atomic Charges (esu) vs. Dielectric Constant ϵ	44
XV. Changes in Atomic Charges (esu) with respect to $\epsilon = 1$	45
XVI. Dipole Moments (Debye) of RDX	45

Table	Page
XVII. Absolute Energy and Zero-Point Energy	46
XVIII. Temperature-Corrected (323 K) Thermodynamic Functions (kcal/mole)	46

LIST OF FIGURES

Figure	Page
1. Three Dimensional view of the RDX Molecule	4
2. The RDX molecule. Structure A labels the angles and structure B labels the bonds.	5
3. Carbon–hydrogen bond lengths (Å) vs. dielectric constant ϵ . The equilibrium bond–lengths of H18–C3 (\diamond), H16–C1 (Δ), and H21–C5 (\star) approach limiting values. H18–C3 and H16–C1 are overlapped as expected from symmetry.	21
4. Nitrogen–nitrogen bond lengths (Å) vs. dielectric constant ϵ . The equilibrium bond–lengths of N7–N6 (\diamond), N10–N4 (Δ), and N13–N2 (\star) approach limiting values. N7–N6 and N10–N6 are overlapped as expected from symmetry.	22
5. IR Stick Spectra of RDX for various values of ϵ . (A) $\epsilon = 1$; (B) $\epsilon = 5$; and (C) $\epsilon = 40$. The scale on the right panels are larger than those on the right.	23
6. Raman Stick Spectra of RDX for various values of ϵ . (A) $\epsilon = 1$; (B) $\epsilon = 5$; (C) $\epsilon = 40$. The scale on the right panels are larger than those on the right.	24
7. IR Intensities of RDX Frequencies ν_{49} , ν_{50} , ν_{51} vs. dielectric strength ϵ . The intensity changes of ν_{49} (\diamond), ν_{50} (Δ), and ν_{51} (\star) approach limiting values near $\epsilon = 20$	25
8. IR Intensities of RDX Frequencies ν_{52} , ν_{53} , ν_{54} vs. dielectric strength ϵ . The intensity changes of ν_{52} (\diamond), ν_{53} (Δ), and ν_{54} (\star) approach limiting values near $\epsilon = 20$	26
9. Raman Intensities of RDX Frequencies ν_{49} , ν_{50} , ν_{51} vs. dielectric strength ϵ . The intensity changes of ν_{49} (\diamond), ν_{50} (Δ), and ν_{51} (\star) approach limiting values near $\epsilon = 20$	27

10. Raman Intensities of RDX Frequencies ν_{52} , ν_{53} , ν_{54} vs. dielectric strength ϵ . The intensity changes of ν_{52} (\diamond), ν_{53} (Δ), and ν_{54} (\star) approach limiting values near $\epsilon = 20$ 28
11. The Z component (\diamond) and Total (Δ) Dipole Moments of RDX verses ϵ . The dipole moments approach limiting values around $\epsilon = 20$. Note the symbols are overlapped. 29
12. Thermodynamic Properties of RDX vs. dielectric strength ϵ . $T\Delta S$ (Δ); ΔH (\diamond); and ΔG (\star) approach limiting values near $\epsilon = 20$ 30

CHAPTER I

Introduction

The physical phenomenon of solubility is often reduced to the rule of thumb, “like dissolves like.” This rule is a helpful guideline for predicting solubility, but it fails to provide detailed insight to the interesting problem of solvation. Until recent years, insight into the detailed molecular interactions in solutions were not amenable to either experimental or theoretical studies of microscopic phenomena.

Recent advances in laser spectroscopy have allowed for real-time studies of dynamical processes in solution[1] and, given advances in supercomputers, theoretical treatments of the chemical and physical processes occurring in solution are being developed[2]. The advances in theory and experiment are leading to comprehensive descriptions of the physical and chemical phenomena occurring in solution-phase chemistry, however, there remains much to be understood.

The ideal theoretical treatment of solutions requires full-dimensional quantum mechanical dynamics calculations. These calculations, even with the recent developments in supercomputers, are impractical. A less sophisticated method would be to treat the solute quantum mechanically while treating the solvent molecules classically. Again the computational demands limit studies to small solute molecules. The computational demands mandate that, approximations need to be made in order to study the solvation of a moderately sized compound in detail. Less sophisticated continuum solvation models are being employed in studies that cannot be treated in greater detail due to the complexity of the system[3–5]. These models treat the solvent as a dielectric continuum, eliminating an explicit description of the solvent molecules and decreasing the computational demands. Substantial improvements to the models have been made by allowing the solute

molecules to be treated either classically or quantum mechanically. Such models have been shown, after adequate parameterization, to predict solvation free energies comparable to those predicted from the more rigorous simulations that explicitly include the solvent molecules[5]. Using a continuum model of solvation, the effects of the solvent dielectric constant on the geometries, vibrational frequencies, infrared and Raman spectra and charge distributions of hexahydro-1,3,5-trinitro-1,3,5-triazine (RDX) are calculated.

Hexahydro-1,3,5-trinitro-1,3,5-triazine (RDX), illustrated in Figures 1 and 2, has a central six-membered ring consisting of alternating carbon and nitrogen atoms. Nitro groups are bound to the ring nitrogens while hydrogens are bound to the carbons. Due to the large size of RDX, (fifteen heavy atoms as well as six hydrogens) only lower level *ab initio* treatments such as Hartree-Fock are practical.

The explosive RDX is a major component of propellants used by the Department of Defense (DoD). The DoD has large stockpiles of such propellants, which consist of RDX, binder and filler, that often become unstable over time. It is of interest to extract the RDX from the propellant mixtures for recycling; however, common solvents necessary to efficiently remove the RDX from the propellants are toxic and environmentally unacceptable. Thus, there has been strong interest in developing environmentally acceptable methods of extracting RDX from propellant grains. One approach has been to extract RDX with supercritical carbon dioxide (SF CO₂).

Unfortunately, RDX has low solubility in SF CO₂. The experiments of Morris et al.[6] however, have shown improved solubility of RDX when the SF CO₂ is doped with as little as 4% of a polar modifier. Virtually nothing is known about what the modifier does to the solvent-solute interaction that increases solubility. Therefore, an ultimate goal is to determine the characteristics of the polar modified SF CO₂ that control the solubility of RDX. In order to arrive at such determinations, the types of interactions occurring between the solvent and solute, including changes that take place in both the solvent and the RDX molecules due to their interactions need to be understood.

One can imagine two limiting case models of RDX + Polar Modifier (PM) in SF CO₂. In the first case, the RDX and PM are distributed evenly throughout the SF CO₂. The second case has the RDX surrounded by one or more solvation shells of the PM, and this complex is then miscible in the SF CO₂. The model represented in this study is best associated with a solution of dilute RDX in a neat polar solvent, which is analogous to the second limiting case described above. The results and analyses described in this study will proceed with this in mind.

This study is a first step toward developing a theoretical chemical model to study the interactions and changes of the solute molecule due to a polar solvent. The model, described below, is based on Onsager's reaction field theory of studying solvent effects[7,8]. The Onsager model is a very simple one wherein the solute molecule sits inside an empty spherical cavity, that is surrounded by a solvent with a uniform dielectric constant. The questions this study will attempt to answer include: 1) What is the dependence of the Gibbs free energy on the polarity and polarizability of the solvent, represented here by the solvent's dielectric constant? 2) What changes occur in RDX as the solvent's dielectric constant increases? 3) Are any of these changes useful in explaining the changes in the Gibbs free energy? 4) Can the calculated molecular properties of RDX in a dielectric medium suggest experiments that might further the understanding of the RDX/solvent interactions? 5) Do these calculations suggest deficiencies in using such a low level of theory to model solvent effects? These issues will be addressed below using the results of *ab initio* calculations of the molecular properties of an RDX molecule in the presence of a solvent reaction field.

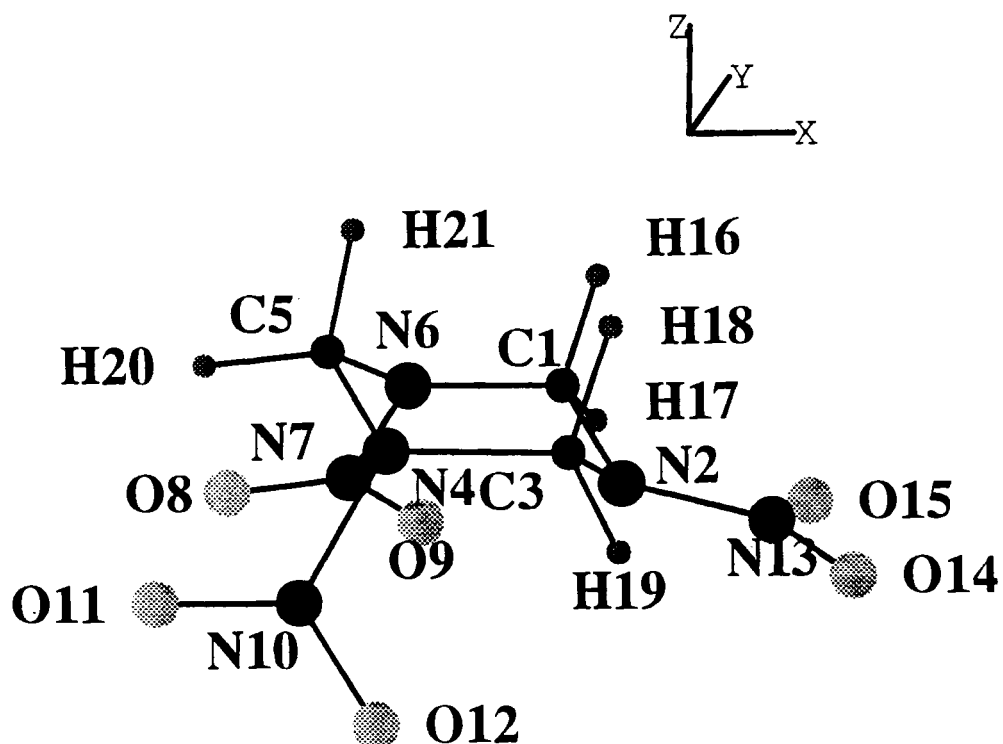


Figure 1. Three Dimensional view of the RDX molecule.

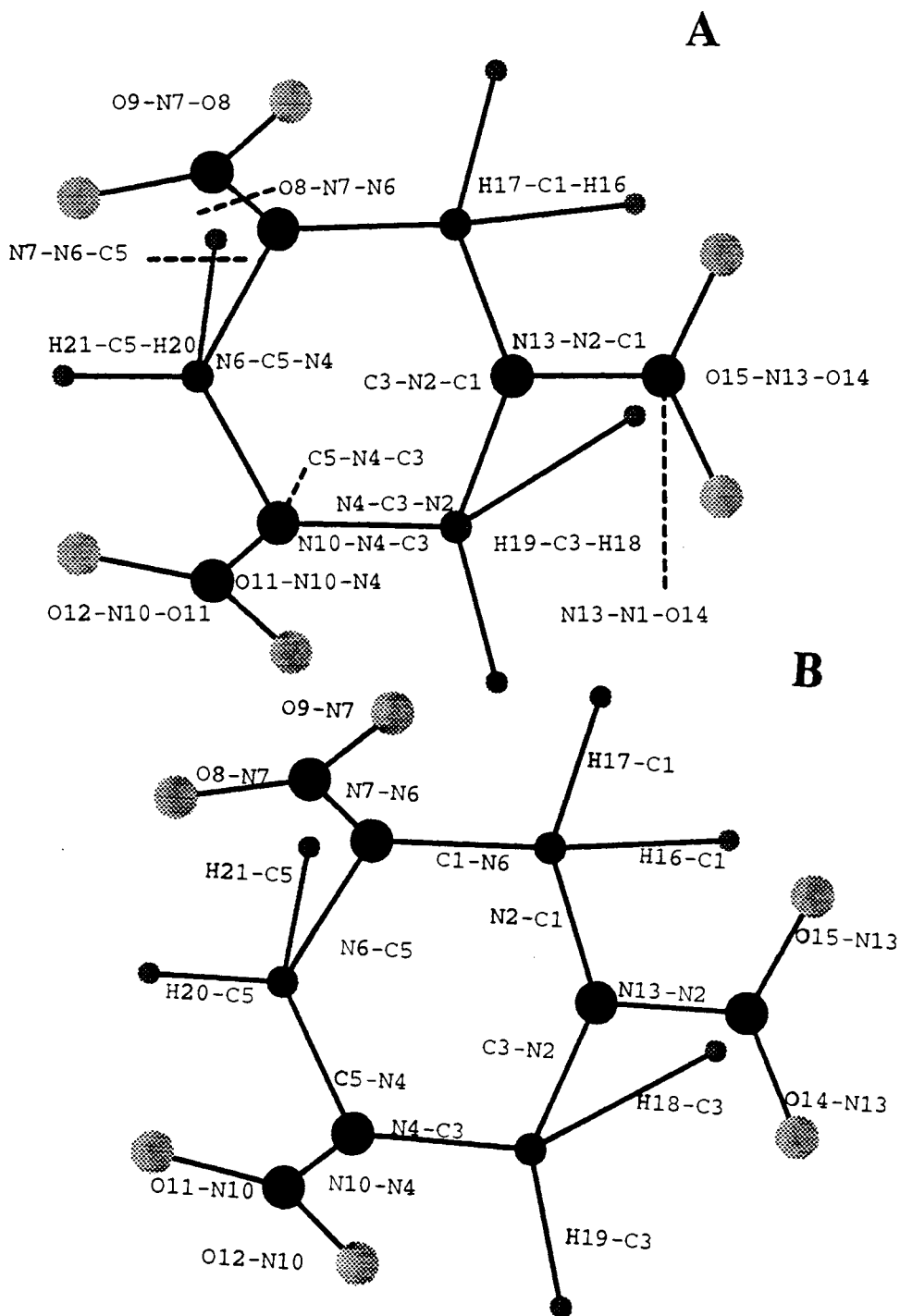


Figure 2. The RDX molecule. Structure A labels the angles and structure B labels the bonds.

The first term of Eqn. 2 is the electron kinetic energy operator for electron "1." The second term is the potential energy operator for electron "1" being attracted to all of the α nuclei with charges Z_α . The coulomb operator $J_j(1)$ gives the potential for electron "1" being repelled by the remaining j electrons. $K_j(1)$ The exchange $K_j(1)$ operator results from the requirement that the wave function be antisymmetric with respect to electron exchange.

The definitions of the coulomb repulsion operator, $J_j(1)$ and the exchange operators, $K_j(1)$ are:

$$J_j(1)\Psi_i(1) = \left[\int \Psi_j(2) \frac{1}{r_{12}} \Psi_j(2) dv_2 \right] \Psi_i(1) \quad (3)$$

$$K_j(1)\Psi_i(1) = \left[\int \Psi_j(2) \frac{1}{r_{12}} \Psi_i(2) dv_2 \right] \Psi_j(1). \quad (4)$$

The Ψ_i are molecular orbitals (MOs) that are obtained by solving the HF-SCF equation and represent a wave function for one electron. The MOs are approximated mathematically as a linear combination of atomic orbitals (LCAO).

$$\Psi_i = \sum_k c_{ik} f_k. \quad (5)$$

The functions f_k are the atomic orbitals. The complete set of c_{ik} are known as the MO coefficients, and the determination of these coefficients is the purpose of solving the HF-SCF equations.

The wave function, Ψ_i , is solved iteratively. That is, an initial set of c_{ik} is chosen. The exchange and coulomb operators are calculated, and then the HF-SCF equation is solved for a new set of c_{ik} . The new set replaces the initial set and the process is repeated until convergence is achieved. Convergence of the HF-SCF equations is obtained when the largest change in MO coefficients is less than 1×10^{-8} . The MOs are then used to calculate the properties of RDX.

Onsager Theory

Onsager theory [7,8] can be used to predict the effects of the solvent on the solute molecule RDX. Onsager's theory was developed in order to improve Debye's

formula for the dielectric constant, ε :

$$\frac{\varepsilon - 1}{\varepsilon + 2} = \frac{4\pi}{3} \sum N \left(\alpha + \frac{\mu^2}{3kT} \right). \quad (6)$$

The thermal energy is kT , μ is the permanent dipole, N is the concentration, and α is the polarizability of the species. The sum is extended over all species present in the solution.

Onsager[7] began with the same molecular model as Debye, that the polarizability of the molecule, α , is related to an “internal refractive index” n by

$$\alpha = \frac{n^2 - 1}{n^2 + 2} a^3, \quad (7)$$

where a is the radius of a spherical molecule. Given an electric field \vec{F} and a unit vector \vec{u} , in the direction of the permanent dipole moment, the total electric moment \vec{m} , of the molecule is

$$\vec{m} = \mu_0 \vec{u} + \alpha \vec{F}. \quad (8)$$

Consider a point dipole \vec{m} inside a spherical cavity of radius a immersed in an unpolarized medium of dielectric strength ε . The electric potential Φ must satisfy Laplace’s equation,

$$\nabla^2 \Phi = 0 \quad (9)$$

with boundary conditions

$$\Phi(r, \theta) - \frac{\vec{m} \cos \theta}{r^2} = \text{continuous} < \infty, \quad (10)$$

and

$$\left(\frac{\partial \Phi}{\partial r} \right)_{r=a-0} = \varepsilon \left(\frac{\partial \Phi}{\partial r} \right)_{r=a+0}. \quad (11)$$

The solutions to Laplace’s equation are:

$$\Phi = \frac{\vec{m} \cos \theta}{r^2} - \vec{R}r \cos \theta, \quad (r < a) \quad (12)$$

and,

$$\Phi = \frac{\vec{m}^* \cos \theta}{\varepsilon r^2}, (r > a). \quad (13)$$

The symbols \vec{m}^* and \vec{R} are defined as:

$$\vec{m}^* = \frac{3\varepsilon}{2\varepsilon + 1} \vec{m} \quad (14)$$

and

$$\vec{R} = \frac{2(\varepsilon - 1)}{2\varepsilon + 1} \frac{\vec{m}}{a^3}. \quad (15)$$

The reaction field \vec{R} is physically the field due to the dipole \vec{m} enhanced by the dielectric medium.

Self-Consistent-Reaction Field

Hartree-Fock Self-consistent-field theory and Onsager theory are combined by treating Onsager theory as a perturbation to the HF-SCF equations to give the Hartree-Fock Self-consistent-reaction-field (HF-SCRF) equation[11]:

$$H_{RF}(1)\Psi_{RF}(1) = E_{HF}\Psi_{RF}(1). \quad (16)$$

where the operator H_{RF} is defined as,

$$H_{RF}(1) = H_{HF}^0(1) + H^1(1). \quad (17)$$

The operator, H_{HF}^0 is the HF-SCF operator defined in equation 2. The perturbation from Onsager, H^1 couples the dipole of the molecule to the solvent continuum and is defined as:

$$H^1 = \hat{\vec{\mu}} \cdot \vec{R}, \quad (18)$$

where $\hat{\vec{\mu}}$ is the electric dipole moment operator $\hat{\vec{\mu}} = (ix + jy + kz)$, and \vec{R} is the reaction field from Onsager Theory[7],

$$\vec{R} = \frac{2(\varepsilon - 1)}{2\varepsilon + 1} \frac{\vec{\mu}}{a_0^3}. \quad (19)$$

The solvent dielectric constant is ϵ , $\vec{\mu}$ is the electric dipole moment vector of the solute,

$$\vec{\mu} = \int \Psi_{RF}^* \hat{\vec{\mu}} \Psi_{RF}, \quad (20)$$

and a_0 is the radius of the cavity in which the solute sits. Like in the HF-SCF method, H^1 , is dependent on the wave function needing to be calculated. The HF-SCRF equation is solved the same way the HF-SCF is solved. The solution to the HF-SCRF equation is a wavefunction for the solute which interacts with the solvent.

CHAPTER II

Theory

A thermodynamic model for predicting the relative solubility of RDX in modified SF CO₂ should predict the change in free energy resulting from dissolving RDX crystals in SF CO₂ doped with polar modifiers. From a practical standpoint, this requires the breaking of the problem into parts, solving each part, and re-assembling those parts to make a whole solution. This study is one of the parts required for understanding the solvation of RDX in CO₂ with polar modifiers. The change in free energy, ΔG , of dissolving RDX in the modifier, is calculated. In other words, this study examines ΔG of solvation as a function of the dielectric constant ϵ of a solvent. This study also examines the geometry, and frequencies, charge distributions, IR and Raman spectral intensities, and the changes in each of these properties of the solute molecule, RDX.

Hartree-Fock Theory

Hartree-Fock Self-consistent-field (HF-SCF) methods are used in order to obtain the structure, frequencies, energies, and charge distributions of the solute molecule RDX. The HF-SCF equation is made up of a one-electron operator, H_{HF}^0 , acting upon a one-electron wave function Ψ_i [9,10]:

$$H_{HF}^0(1)\Psi_i(1) = E_i\Psi_i(1), \quad (1)$$

where E_i is the eigenvalue of the Hartree-Fock Hamiltonian operator, H_{HF}^0 :

$$H_{HF}^0(1) = -\frac{1}{2}\nabla_1^2 - \sum_{\alpha} \frac{Z_{\alpha}}{r_{1\alpha}} + \sum_j [2J_j(1) - K_j(1)]. \quad (2)$$

CHAPTER III

Details of the Calculations

The Gaussian-92 set of computer codes[12] used in the SCRF calculations were designed to be used by the non-expert in quantum chemical calculations. This user-friendly set of computer codes enables the non-expert to focus on the chemical problem being studied rather than the details of performing the calculations. The two types of HF-SCRF calculations that will be presented here are a series of geometry optimizations of the RDX molecule as a function of increasing dielectric constant and subsequent calculations of the vibrational frequencies of the optimized molecule at each value of the dielectric constant. All inputs are free-format and mnemonic.

Geometry Optimization and Frequency Calculations

The initial geometry corresponds to the molecular structure determined from crystallographic neutron diffraction measurements[13]. This structure, the chair form, is shown in Fig. 1. RDX may also exist in the boat conformation; however, due to a lack of measured molecular structure information, that conformation is not studied here. There are no experimental data for RDX in solution, however, it is reasonable to assume the crystalline and solution conformations are similar. Thus, the experimental crystal structure is used for an initial guess in the calculation. This initial structure is then optimized in the presence of the reaction field perturbation for each value of the dielectric constant, ϵ . The structures are assumed to be optimized (i.e., to the equilibrium geometry) when all the default convergence criteria are met in the Gaussian-92 codes. The two criteria that define an equilibrium stable structure are based on the first and second derivatives

of the energy. Convergence is assumed to occur when the largest first derivative of the energy with respect to any single internal coordinate is less than 4.5×10^{-4} hartrees/bohr. To characterize the nature of this critical point, a normal mode analysis must be performed; this requires the second derivatives of the energy with respect to displacements of the nuclear coordinates at the optimized geometry. Diagonalization of the $3N \times 3N$ energy second derivative matrix yields $3N$ eigenvectors, six of which have eigenvalues equal to zero (which correspond to the translational and rotational modes) and $3N - 6$ non-zero eigenvalues (which correspond to harmonic vibrational frequencies) at equilibrium. All structures presented in this study have the required six zero frequencies and the $3N - 6$ positive non-zero frequencies.

Each harmonic vibrational frequency is observable by either IR or Raman spectroscopy. Those observable through IR spectroscopy are termed as “IR active” while those observable through Raman spectroscopy are termed as “Raman active”. The IR intensity I of a frequency is related to the intensity of the incident radiation of the same frequency I_0 by

$$I = I_0 e^{-CLA}, \quad (21)$$

where C is the concentration and L is the pathlength. The absorption coefficient A is approximated as

$$A = \frac{\pi N g}{3000 c^2 \times 2.302581} \left| \frac{\partial \mu}{\partial Q} \right|^2, \quad (22)$$

where N is Avagadro’s number, g is a degeneracy factor, c is the speed of light, μ is the dipole moment and Q is a normal coordinate corresponding to the vibrational frequency.

The Raman intensity I of an eigenfrequency ν is related to the frequency of the incident radiation ν_i by

$$I = \left(\frac{16\pi^4 \nu_i^4}{3c^3} \right) (\mu_{ind})^2, \quad (23)$$

where the induced dipole moment μ_{ind} is given by the polarizability of the molecule α described by the Taylor expansion $\alpha = \alpha_0 + \left(\frac{\partial \alpha}{\partial Q} \right)_0 Q + \dots$, the time dependent

electric field of the incident radiation $E = E_0 \cos(2\pi\nu_i t)$ and a constant B by

$$\mu_{ind} = \alpha_0 E_0 \cos 2\pi\nu_i t + \frac{BE_0}{2} \left(\frac{\partial\alpha}{\partial Q} \right)_0 \times [\cos 2\pi(\nu_i + \nu)t + \cos 2\pi(\nu_i - \nu)t]. \quad (24)$$

The 6-31G* basis set was used for the calculations[14-17]. The geometry of the molecule was optimized for each value of the solvent dielectric constant using the analytical first derivatives of the energy with respect to changes in nuclear coordinates. All the optimized geometries have gradients of the energy less than 4.5×10^{-4} (hartrees/bohr) commensurate with the default convergence criteria in Gaussian-92.

This study also used the default method in Gaussian-92 for estimating the cavity radius a_0 . In this prescription[18], the cavity radius is determined by making certain that the boundary of the cavity includes all regions of space surrounding the molecule where the HF-SCF electron density is greater than 0.001 electrons/bohr³. This volume is referred to as the Density Envelope[18] (DE). It has been found that for a large number of organic molecules the ratio of the DE to the experimental volume is nearly the constant value of 0.75[18]. Thus, the procedure for estimating a_0 is to calculate the radius of the DE and scale by 1.33. The value of 0.5Å is added to the new radius in order to account for the van der Waal's radius of the solvent molecules. This procedure allows one to estimate a_0 for a molecule for which the volume is not known.

Free Energy Calculations

In addition to determining changes in structure and vibrational frequencies of the RDX molecule due to the solvent field, changes in the Gibbs free energy are calculated at 323 K, the temperature at which the experiments of Morris et al.[6] were conducted.

The Gibbs free energy change ΔG is

$$\Delta G = \Delta H - T\Delta S, \quad (25)$$

where ΔS is the entropy change, ΔH is the enthalpy change and T is the temperature. The free energy of solvation, ΔG_{sol} , is given by,

$$\Delta G_{sol} = H_{\epsilon} - H_{\epsilon=1} - T(S_{\epsilon} - S_{\epsilon=1}), \quad (26)$$

where the subscript ϵ indicates the dielectric constant of the solvent. The absolute entropies and absolute enthalpies are obtained from statistical mechanics[19]. The entropy of a molecule is

$$S = S_{tr} + S_{rot} + S_{vib} + S_{el}, \quad (27)$$

where S_{tr} , S_{rot} , S_{vib} , and S_{el} are the entropies of translation, rotation, vibration, and electronic degeneracy respectively. The entropy of translation, S_{tr} , is given by

$$S_{tr} = k \ln \left(\frac{2\pi M k T}{h^2} \right)^{\frac{5}{2}} V + \frac{3}{2} \quad (28)$$

where M is the total mass of the molecule, V is the molecular volume, and k and h are Boltzmann's and Planck's constants, respectively. The entropy of rotation, is

$$S_{rot} = k \ln \left\{ \frac{\pi^{\frac{1}{2}}}{\sigma} \left(\frac{8\pi^2 k T}{h^2} \right)^{\frac{3}{2}} I_A^{\frac{1}{2}} I_B^{\frac{1}{2}} I_C^{\frac{1}{2}} \right\} + \frac{3}{2}, \quad (29)$$

where I_A , I_B , and I_C are the principle moments of inertia (for an asymmetric top molecule such as RDX), and σ is the rotational symmetry number (for RDX $\sigma = 1$). The entropy of electronic degeneracy is given by

$$S_{el} = k \ln \omega_{ei}, \quad (30)$$

where ω_{ei} is the degeneracy of the electronic state (in this case, $\omega_{ei} = 1$). The entropy of vibration is

$$S_{vib} = k \sum_i \left\{ \left(\frac{u_i}{e^{u_i} - 1} \right)^{-1} - \ln (1 - e^{-u_i}) \right\}. \quad (31)$$

where

$$u_i = \frac{h\nu_i}{kT} \quad (32)$$

and ν_i is the vibrational frequency of the molecule.

The enthalpy, $H = E + pV$, is corrected to a given temperature T by[19],

$$\Delta H(T) = H(T) - H(0) = H_{trans}(T) + H_{rot}(T) + \Delta H_{vib}(T) + kT, \quad (33)$$

where

$$H_{trans}(T) = H_{rot}(T) = \frac{3}{2}kT \quad (34)$$

and

$$\Delta H_{vib}(T) = H_{vib}(T) - H_{vib}(0) = h \sum_i \frac{\nu_i}{e^{u_i} - 1}. \quad (35)$$

CHAPTER IV

Results and Discussion

Geometry

The equilibrium geometries for RDX solvated in media of different dielectric constants are given in Tables I–III. Fifty seven internal coordinates are needed in order to uniquely describe the RDX molecule. One redundant coordinate, C1–N6, has been added to Table I (which gives the values of the bond lengths for various values of the dielectric constant), in order to “close the ring.” Tables II and III give the values of the bond angles and torsional angles, respectively. The atoms are as labeled in Fig. 1. The bonds and bend angles are as labeled in Fig. 2.

The reference values used are those of the gas-phase ($\epsilon = 1$). Changes in geometric parameters, with increasing ϵ , larger than 0.25% of the reference value are reported in Table IV. Few bond lengths satisfy this requirement, however, a few trends are noted.

In the chair conformation, shown in Fig. 1, two of the nitro groups occupy pseudo-axial positions (O12–N10–O11 and O8–N7–O9), and one occupies a pseudo-equatorial position (O15–N13–O14). The term “pseudo-equatorial,” indicates that the nitro group is approximately parallel to the plane formed by the N6–C1–N4–C3 ring atoms. Similarly, the term “pseudo-axial,” indicates that the nitro group is approximately perpendicular to the plane formed by the N6–C1–N4–C3 ring atoms. Therefore, the changes in the geometric parameters corresponding to the type of nitro group differ.

The C–N bonds which contain N4 and N6 (the binding sites of the pseudo-axial nitro groups) increase less than 0.25% with increases in ϵ , while the two C–N bonds that contain N2 (the binding sites of the pseudo-equatorial nitro group)

are shortened by 0.22%. All of the N–N bond lengths, illustrated in Fig. 4, are shortened with increasing ϵ . The N2–N13 bond length changes 0.55%, twice the change of the other two N–N bonds. The N–O bond lengths are all lengthened with increasing ϵ with the bonds O8–N7 and O11–N10 being changed by one fifth the change of the O9–N7 and O12–N10 bonds. This trend is not repeated in the pseudo-equatorial nitro group; both the oxygen atoms are symmetry equivalent. The changes in the C–H bonds are all less than 0.1%. However, the bond lengths H16–C1, H18–C3 and H21–C5 are graphed in Fig. 3 as a function of ϵ in order to help illustrate two points. First, the carbons are not all identical bonding sites.

The second point illustrated, with the help of Fig. 4, is the limit of effectiveness of increasing ϵ . In fact, the change in bond lengths for ϵ varying from one to five, is greater than when ϵ varies from ten to forty.

The changes in the equilibrium bond angles are all less than 1° with one exception. The angle N13–N2–C1 changes by 2.08% or 2.40° . The extension of this angle and the angle C3–N2–N13 indicate a downward movement of N13 relative to N2, keeping the same frame of reference as Fig. 1.

Some of the torsional angles change a great deal as ϵ increases. The changes range in magnitude from 0° to 9.54° , with half of them changing more than 1° . The highest percentage change, 6.42%, is for the torsional change defined by O8–N7–N6–C5 (see Fig. 1). This torsional angle change has the effect of making the torsional angle defined by O8–N7–N6–C1 closer to 180° , defining a plane. By symmetry arguments, O11–N10–N4–C3 must also become more planar, which it does. The largest magnitude change however does not coincide with the largest percent change and is worth noting. The torsional angle N13–N2–C1–N6 changes by -5.72%. This is more evidence of a downward shift of the N13 nitro group as ϵ increases.

Harmonic Vibrational Frequencies

The equilibrium frequencies of RDX solvated in media of different dielectric constants are given in Tables V – VI. The larger relative changes in these frequencies are given in Table VII. Stick spectra are shown in Figures 5. and 6.

The frequencies, like the geometric parameters, change little with increasing dielectric constant. Some of the largest absolute changes in frequencies occur for modes 49–54. The modes 49, 50 and 51 primarily involve motions of the nitro-group nitrogens and change by 12, 16, and 18 cm^{-1} , respectively. Analysis of the normal mode vectors for these three modes indicates that the atoms primarily displaced are the nitro-group nitrogens. The nitrogens move orthogonally to the nitro-group planes. Mode 49 is localized mostly over N13, while mode 50 involves all three nitro-group nitrogens (N13, N10, N7). Mode 51 is more localized, including only the N7 and N10 nitro group nitrogens. The other three modes 52, 53 and 54 involve C–H stretches. Mode 52 is the hydrogen asymmetric stretch mode H16–C1–H18–C3, and 53 is its symmetric stretch partner, H16–C1+H18–C3. Mode 54 is almost entirely H21–C5 stretch. The largest relative change in these six modes is small (less than 1%) and, corresponds to the largest absolute change in frequencies over the entire range of ϵ , approximately 18 cm^{-1} from the gas phase value of 51.

The largest relative change in frequency occurs for 2. The vibrational frequency at $\epsilon = 1$ for this mode is 63 cm^{-1} and the absolute change is 11 cm^{-1} , making a relative change of 18%. This mode involves motions from many atoms and centers upon an umbrella motion of the N2 nitrogen with concomitant motion of the attached atoms C1, C3 and the N13–O14–O15 nitro group.

Infrared and Raman Intensities

The infrared (IR) and Raman spectral intensities exhibit a much stronger dependence on the dielectric strength of the medium. The IR intensities are given as a function of ϵ in Tables VIII and IX. Raman intensities are given as a function

of ϵ in Tables XI and XII. The largest percentage changes in IR and Raman intensities are given in Tables X and XIII, respectively. Both IR and Raman intensities for frequencies $\nu_{49}-\nu_{54}$ are plotted as a function of ϵ in Figs. 7 – 9.

Atomic Charge Distributions and Dipole Moment

The atomic charge distributions are given in Table XIV. The changes in charge distribution relative to $\epsilon = 1$ are given in Table XV. The changes in charge distribution coupled with the changes in the structure of the molecule cause significant changes in the components of the dipole moment of the molecule, which are presented in Table XVI and Fig. 11.

More than 99% of the total dipole moment comes from the z-component, which is perpendicular to the C1–N6–C3–N4 ring atoms. Table XVI also reports the ratio of μ_s/μ_g , where μ_s is the dipole moment in solution ($\epsilon > 1$) and μ_g is the dipole moment of the isolated gas molecule ($\epsilon = 1$). There is a 20% increase in the total dipole moment of $\epsilon = 0$ by the time $\epsilon = 10$. This large increase in dipole moment is due primarily to the higher electron densities on the oxygens below the ring. Figure 11 illustrates that the increase in the dipole moment of the RDX molecule is initially sharp (16% for $\epsilon = 5$), and quickly approaches a limiting value (nearly a 23% increase of dipole moment with increasing ϵ).

According to the Onsager model the influence of the solvent upon the molecule is totally attributable to the interaction of the dipole moment of the molecule with the dipole electric field of the solvent. As noted above, the z-component dominates the total dipole moment. The z-component is ten times larger than the x-component. The y-component of the dipole moment is essentially zero. As expected, the total molecular dipole moment increases as ϵ increases.

Gibbs Free Energy of Solvation

Table XVII gives the HF–SCRF absolute and zero-point vibrational energies of the RDX molecule in solution. The change in the Gibbs free energy of the RDX

molecule as a function of increasing dielectric constant are calculated using the vibrational frequencies (see Equations 25–35). The vibrational frequencies of this study were scaled by 10% for these calculations because the results of ab-initio calculations are generally higher than experimental values.

The results, given in Table XVIII and plotted in Fig. 12, indicate that the Gibbs free energy sharply decreases with the application of the field ($\epsilon = 5$), and continues to decrease, but less rapidly, with increasing ϵ . The entropy change with increasing field is negligible. Therefore, the lowering of the free energy of the system with increasing dielectric constant is due primarily to the lowering of the enthalpy of the system. That the entropy changes are small is not surprising, due to the very small changes in structure and in the harmonic vibrational frequencies. The decrease in the enthalpy of the system, however, can be attributed to the increase in the dipole moment of the RDX molecule in the solution as described above. Both the dipole moment and ΔG curves are almost flat by $\epsilon = 20$ (see Figures 11 and 12).

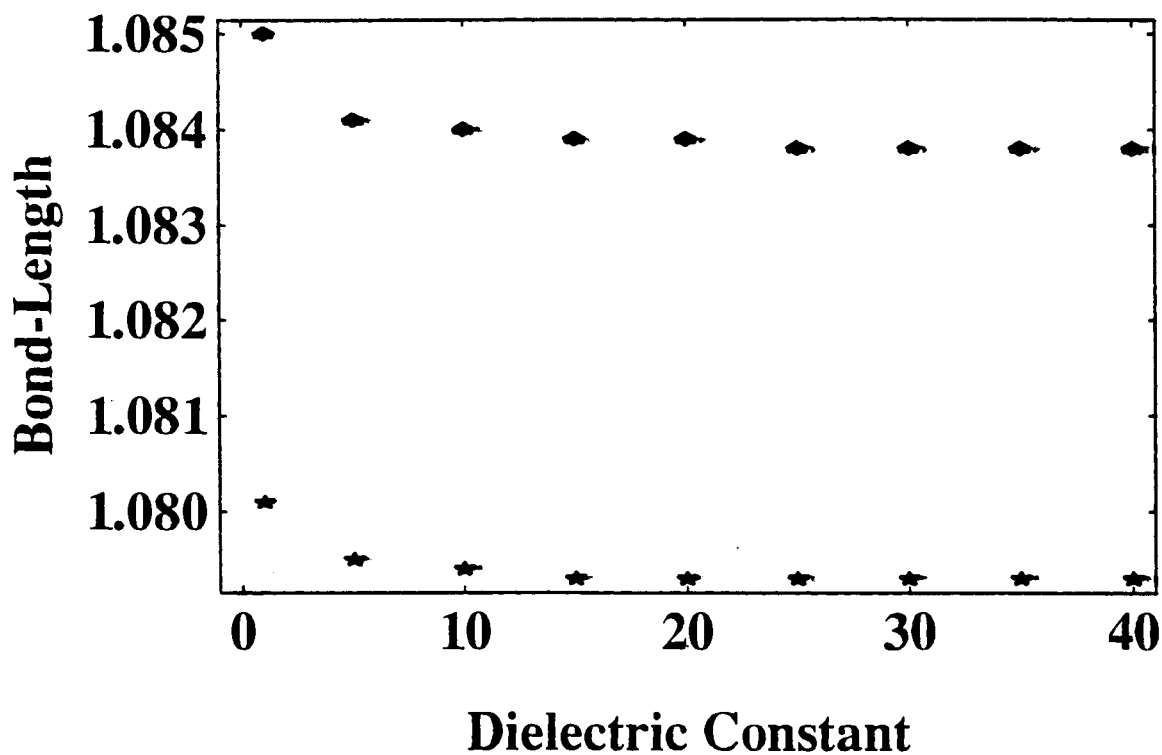


Figure 3. Carbon-hydrogen bond lengths (\AA) vs. dielectric constant ϵ . The equilibrium bond-lengths of H18-C3 (\diamond), H16-C1 (Δ), and H21-C5 ($*$) approach limiting values. H18-C3 and H16-C1 are overlapped as expected from symmetry.

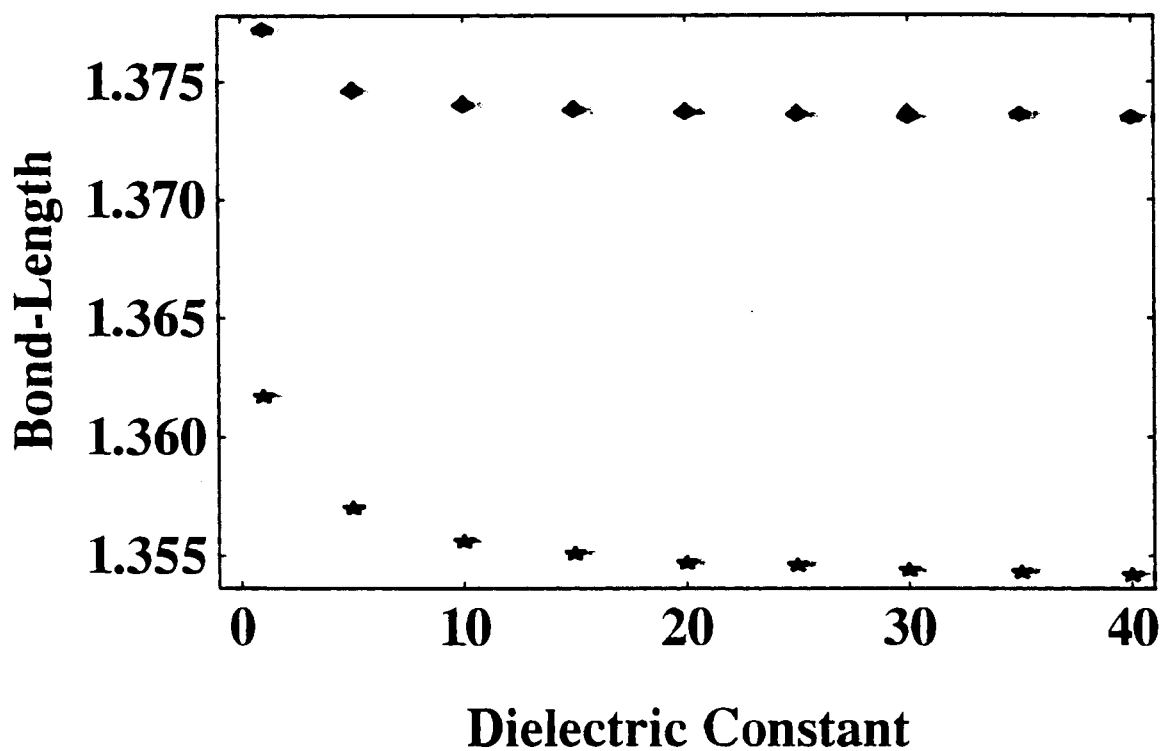


Figure 4. Nitrogen–nitrogen bond lengths (\AA) vs. dielectric constant ϵ . The equilibrium bond-lengths of N7–N6 (\diamond), N10–N4 (\triangle), and N13–N2 (\star) approach limiting values. N7–N6 and N10–N6 are overlapped as expected from symmetry.

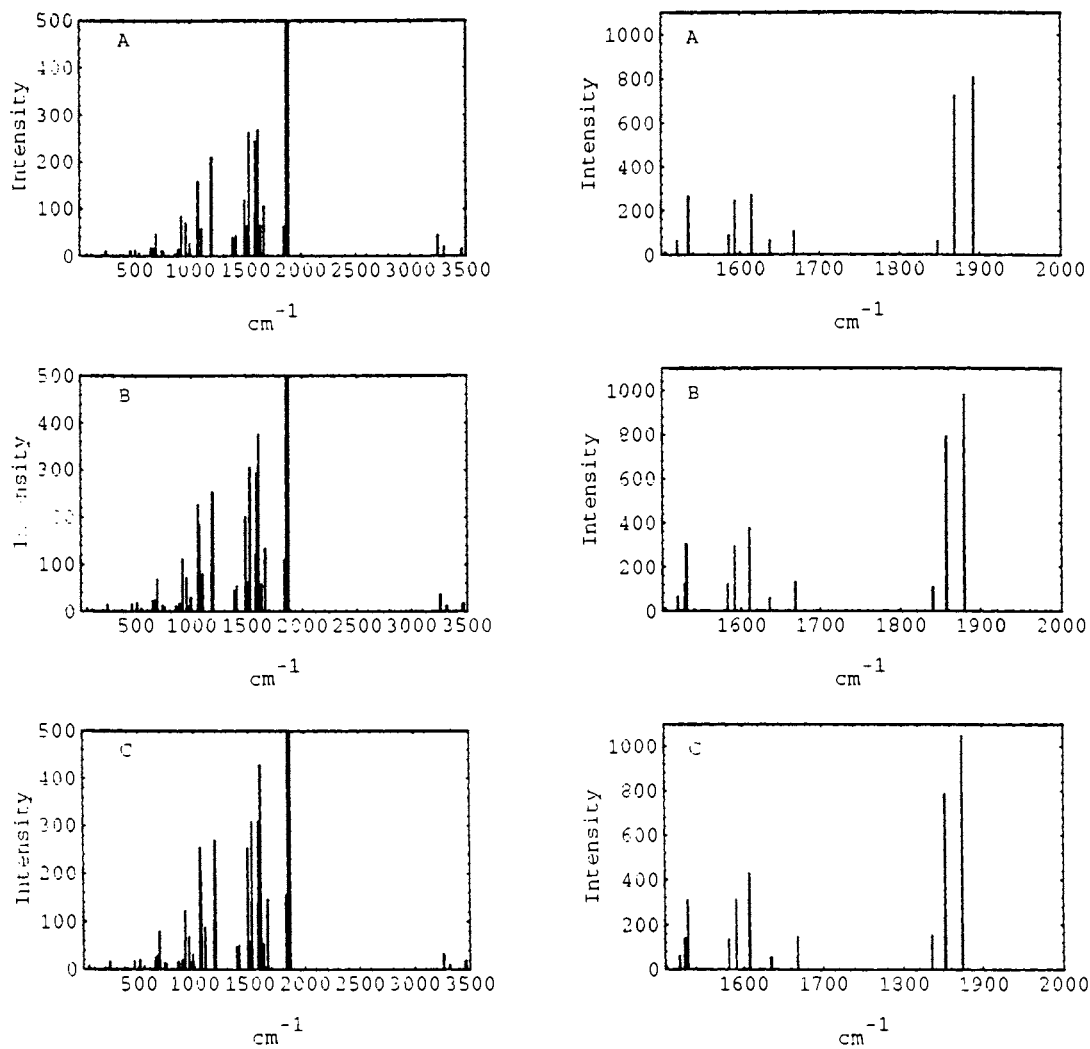


Figure 5. IR Stick Spectra of RDX for various values of ϵ . (A) $\epsilon = 1$; (B) $\epsilon = 5$; and (C) $\epsilon = 40$. The scale on the right panels are larger than those on the left.

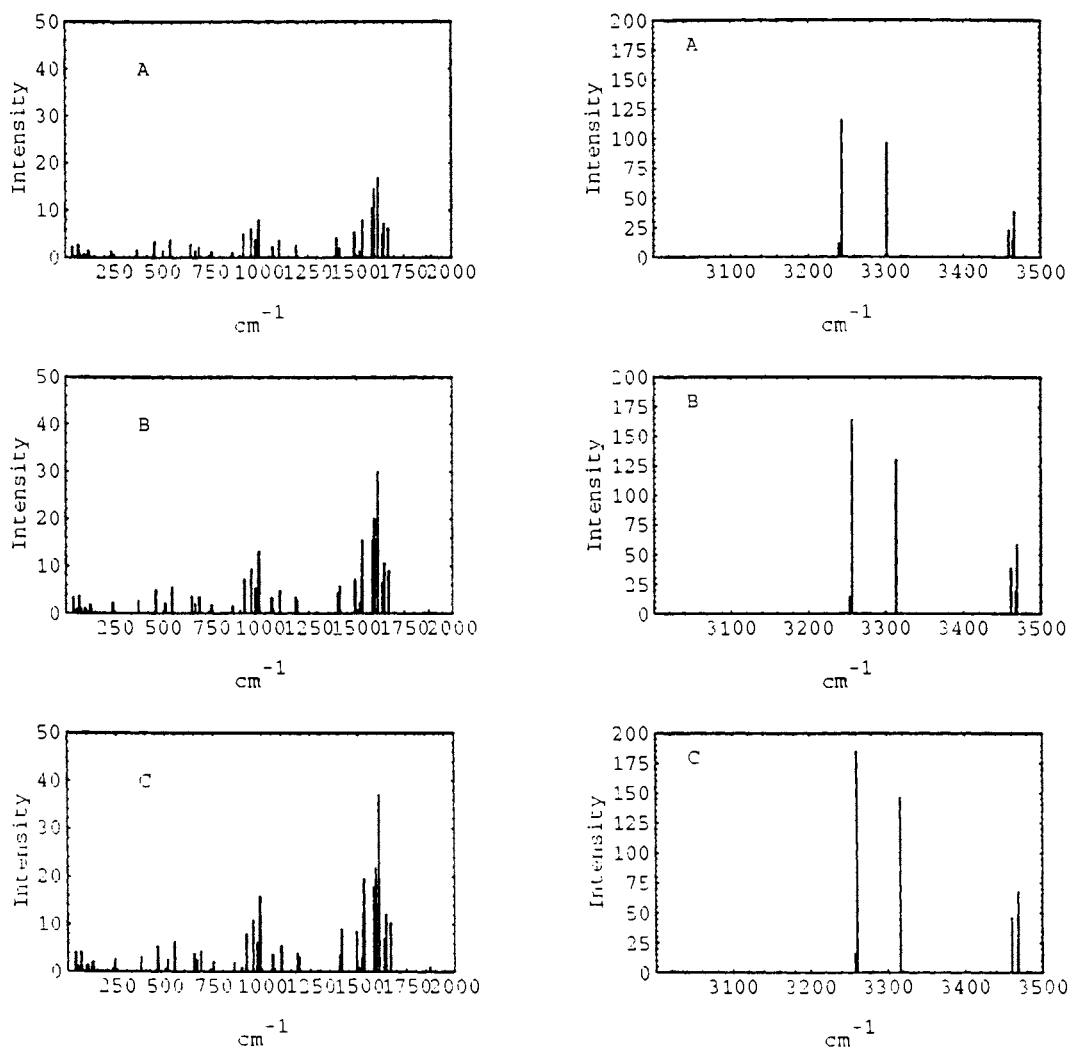


Figure 6. Raman Stick Spectra of RDX for various values of ϵ . (A) $\epsilon = 1$; (B) $\epsilon = 5$; (C) $\epsilon = 40$. The scale on the right panels are larger than those on the left.

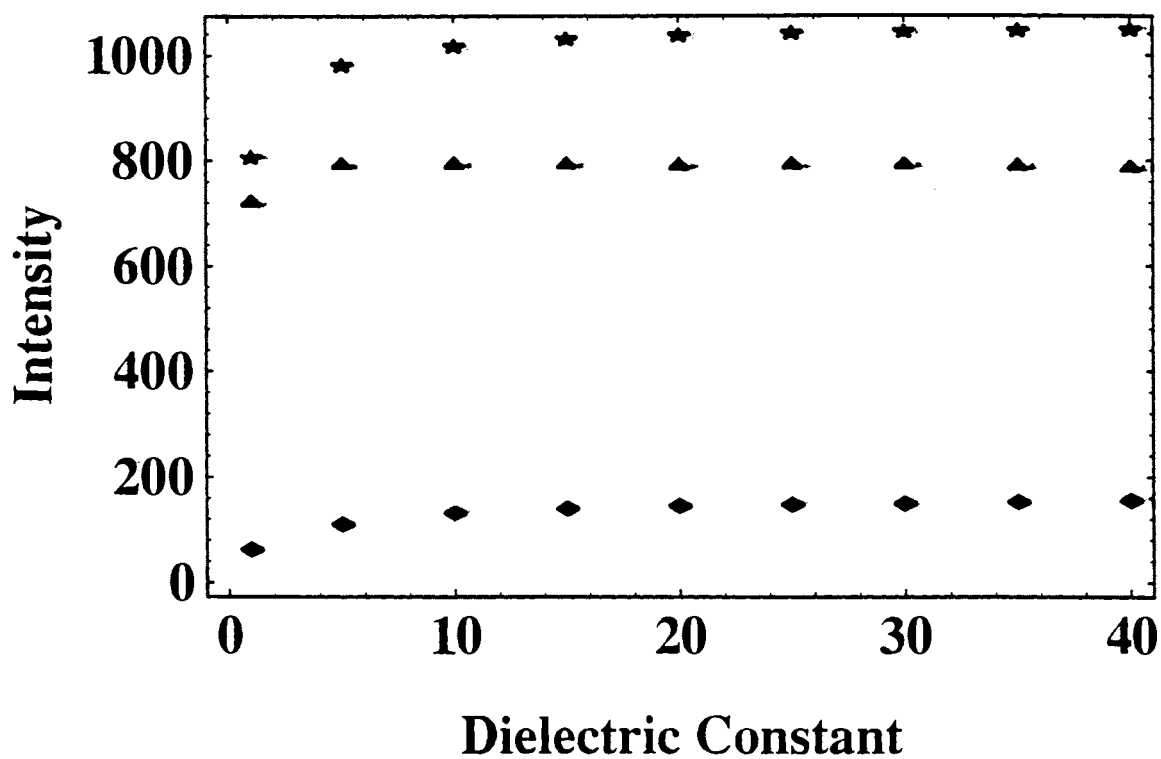


Figure 7. IR Intensities of RDX Frequencies ν_{49} , ν_{50} , ν_{51} vs. dielectric strength ϵ . The intensity changes of ν_{49} (\diamond), ν_{50} (\triangle), and ν_{51} (\star) approach limiting values near $\epsilon = 20$.

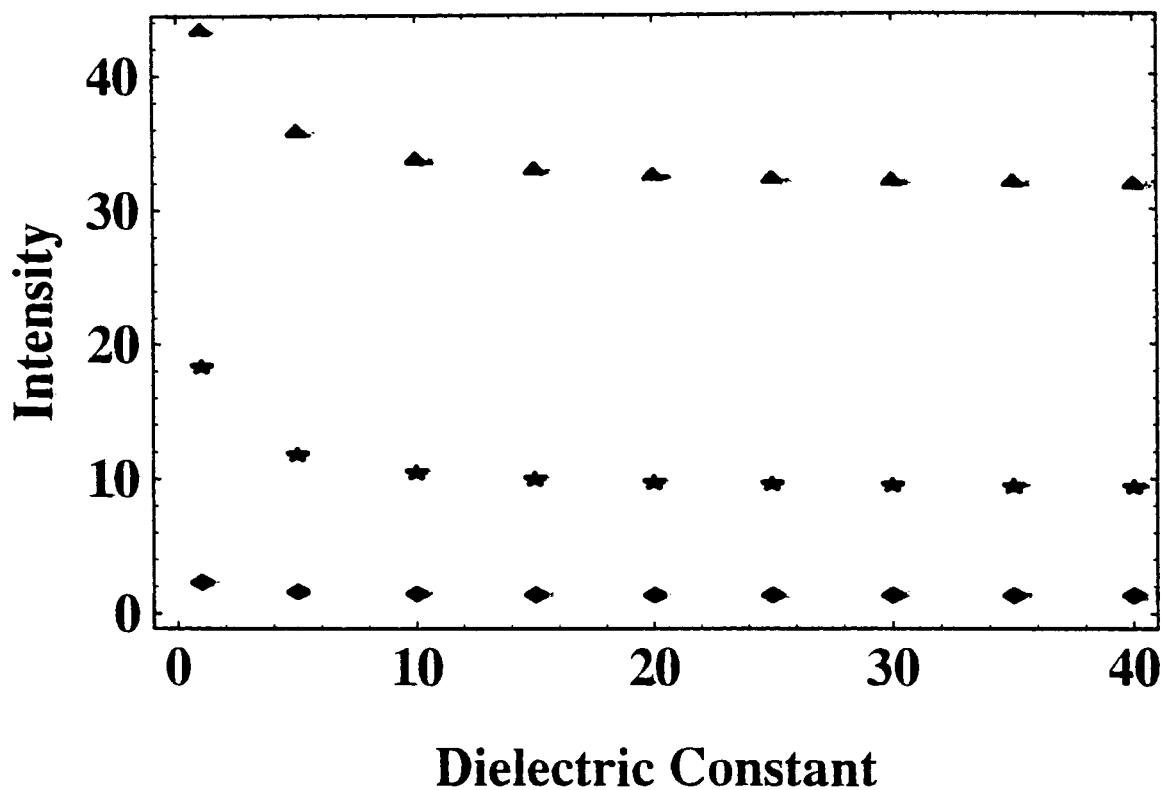


Figure 8. IR Intensities of RDX Frequencies ν_{52} , ν_{53} , ν_{54} vs. dielectric strength ϵ . The intensity changes of ν_{52} (\diamond), ν_{53} (\triangle), and ν_{54} (\star) approach limiting values near $\epsilon = 20$.

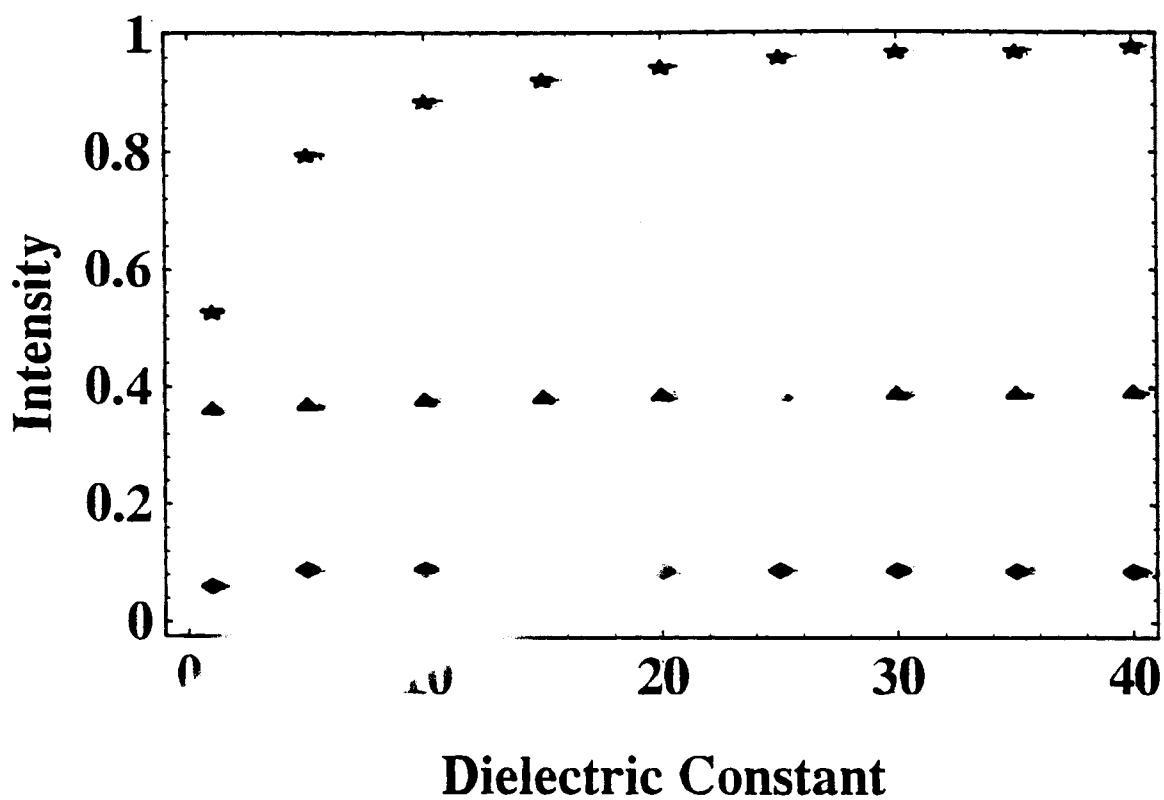


Figure 9. Raman Intensities of RDX Frequencies ν_{49} , ν_{50} , ν_{51} vs. dielectric strength ϵ . The intensity changes of ν_{49} (\diamond), ν_{50} (\triangle), and ν_{51} (\star) approach limiting values near $\epsilon = 20$.

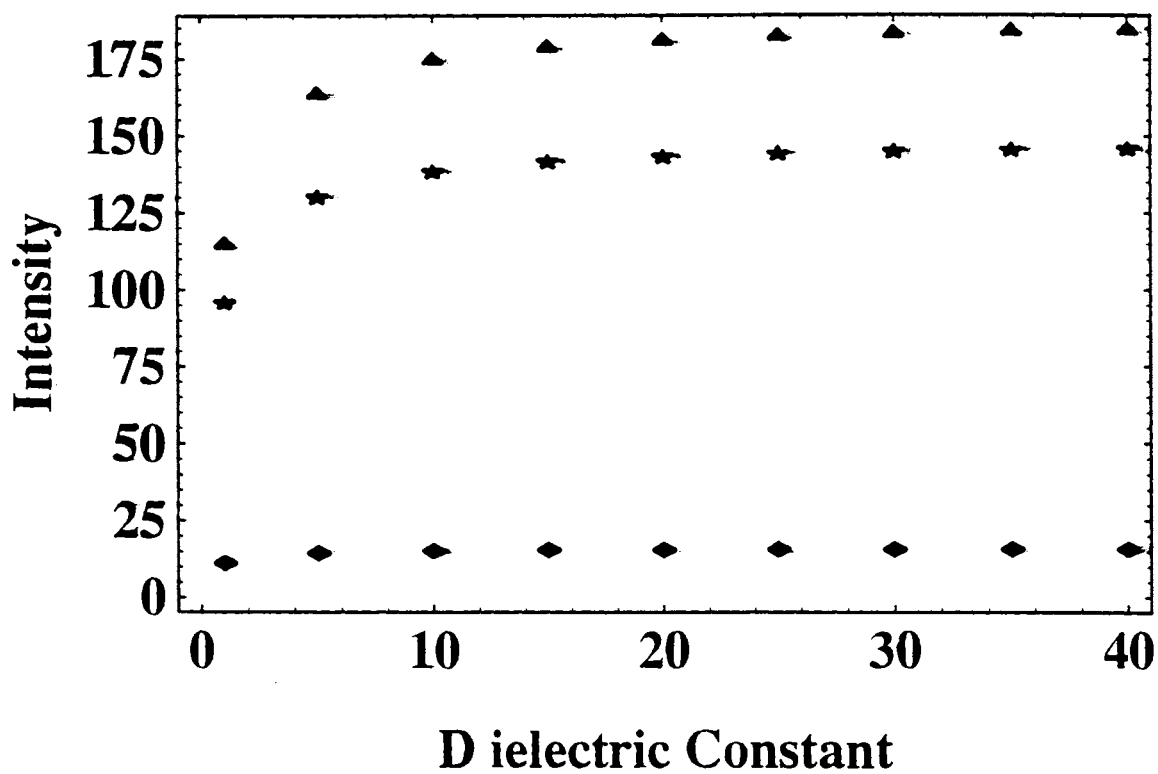


Figure 10. Raman Intensities of RDX Frequencies ν_{52} , ν_{53} , ν_{54} vs. dielectric strength ϵ . The intensity changes of ν_{52} (\diamond), ν_{53} (\triangle), and ν_{54} (\star) approach limiting values near $\epsilon = 20$.

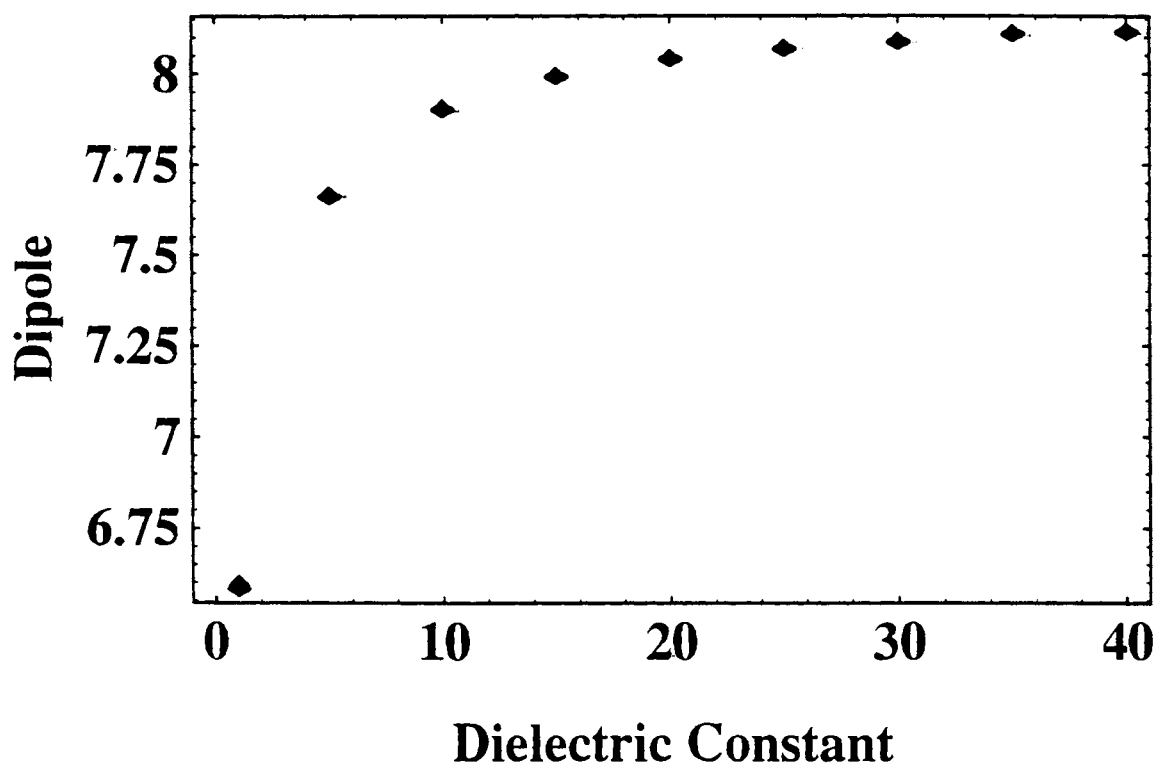


Figure 11. The Z component (\diamond) and Total (\triangle) Dipole Moments of RDX verses ϵ . The dipole moments approach limiting values around $\epsilon = 20$. Note the symbols are overlapped.

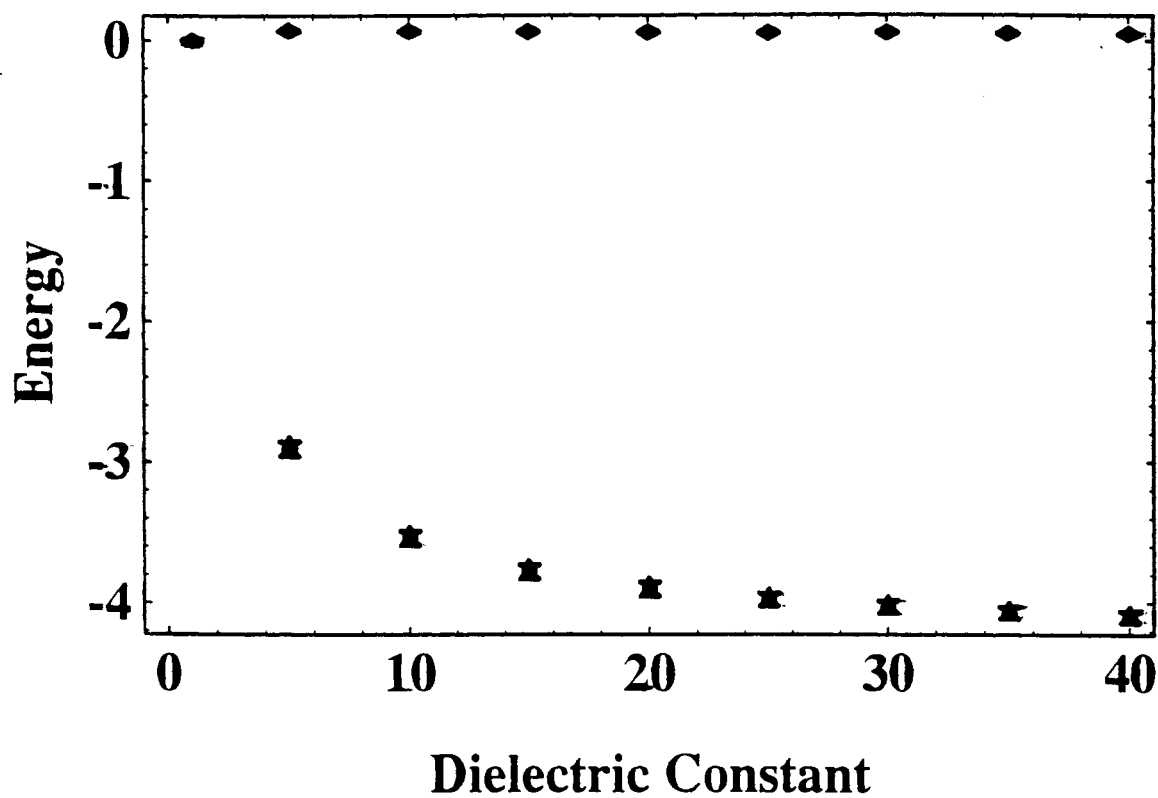


Figure 12. Thermodynamic Properties of RDX vs. dielectric strength ϵ . $T\Delta S$ (\diamond); ΔH (Δ); and ΔG (\star) approach limiting values near $\epsilon = 20$.

TABLE I.

RDX Bond Lengths (\AA) vs. Dielectric Constant ϵ

Coordinate	$\epsilon = 1$	$\epsilon = 5$	$\epsilon = 15$	$\epsilon = 30$	$\epsilon = 40$
N2-C1	1.4643	1.4622	1.4615	1.4612	1.4612
C3-N2	1.4643	1.4622	1.4615	1.4612	1.4612
N4-C3	1.4424	1.4448	1.4456	1.4458	1.4458
C5-N4	1.4529	1.4559	1.4569	1.4571	1.4572
N6-C5	1.4529	1.4559	1.4568	1.4570	1.4572
C1-N6	1.4424	1.4448	1.4451	1.4457	1.4458
N7-N6	1.3772	1.3746	1.3738	1.3735	1.3735
N10-N4	1.3772	1.3747	1.3739	1.3737	1.3735
N13-N2	1.3617	1.3570	1.3551	1.3544	1.3542
O8-N7	1.1874	1.1877	1.1878	1.1878	1.1879
O9-N7	1.1886	1.1905	1.1911	1.1913	1.1913
O11-N10	1.1874	1.1877	1.1878	1.1879	1.1879
O12-N10	1.1886	1.1905	1.1911	1.1913	1.1913
O14-N13	1.1912	1.1918	1.1921	1.1922	1.1922
O15-N13	1.1912	1.1918	1.1921	1.1922	1.1922
H16-C1	1.0850	1.0841	1.0839	1.0838	1.0838
H17-C1	1.0684	1.0683	1.0683	1.0683	1.0682
H18-C3	1.0850	1.0841	1.0839	1.0838	1.0838
H19-C3	1.0684	1.0683	1.0683	1.0683	1.0683
H20-C5	1.0696	1.0696	1.0696	1.0697	1.0697
H21-C5	1.0801	1.0795	1.0793	1.0793	1.0793

TABLE II.

RDX Bond Angles (Degrees) vs. Dielectric Constant ϵ

Coordinate	$\epsilon = 1$	$\epsilon = 5$	$\epsilon = 15$	$\epsilon = 30$	$\epsilon = 40$
H16-C1-N2	110.44	110.49	110.48	110.47	110.46
H17-C1-H16	109.87	109.97	109.99	110.00	110.00
H18-C3-N4	107.19	107.02	106.97	106.98	106.95
H19-C3-H18	109.87	109.97	109.99	110.00	110.01
H20-C5-N6	110.84	110.87	110.86	110.84	110.95
H21-C5-H20	109.96	109.89	109.88	109.86	109.86
C3-N2-C1	115.14	114.82	114.81	114.83	114.82
N4-C3-N2	108.62	108.13	108.01	107.98	107.98
C5-N4-C3	115.25	114.96	114.87	114.85	114.84
N6-C5-N4	111.48	111.33	111.29	111.27	111.27
N7-N6-C5	117.60	117.44	117.40	117.37	117.39
O8-N7-N6	116.53	116.77	116.85	116.85	116.88
O9-N7-O8	126.24	125.90	125.80	125.78	125.74
N10-N4-C3	117.14	116.80	116.71	116.70	116.71
O11-N10-N4	116.53	116.77	116.85	116.85	116.87
O12-N10-O11	126.24	125.90	125.80	125.78	125.75
N13-N2-C1	115.49	117.11	117.67	117.85	117.90
O14-N13-N2	117.01	117.06	117.08	117.09	117.09
O15-N13-O14	125.98	125.86	125.81	125.79	125.79

TABLE III.

RDX Torsional Angles (Degrees) vs. Dielectric Constant ϵ

Coordinate	$\epsilon = 1$	$\epsilon = 5$	$\epsilon = 15$	$\epsilon = 30$	$\epsilon = 40$
N4-C3-N2-C1	54.67	56.46	56.83	56.90	56.93
C5-N4-C3-N2	-51.45	-52.33		-52.56	-52.57
N6-C5-N4-C3	49.86	50.12		50.28	50.29
N7-N6-C5-N4	94.77	93.21	92.77	92.62	92.60
N10-N4-C3-N2	93.38	91.22	90.69	90.56	90.58
N13-N2-C1-N6	166.70	160.33	158.08	157.36	157.16
O8-N7-N6-C5	24.21	25.31	25.66	25.77	25.69
O9-N7-O8-N6	-176.38	-176.71	-176.82	-176.82	-176.85
O11-N10-N4-C3	-168.21	-167.99	-167.95	-167.96	-168.09
O12-N10-O11-N4	176.38	176.71	176.80	176.80	176.84
O14-N13-N2-C1	159.74	161.98	162.94	163.29	163.29
O15-N13-O14-N2	-178.90	-178.21	-178.06	-178.01	-178.02
H16-C1-N2-C3	62.61	60.35	59.86	59.75	59.70
H17-C1-H16-N4	-179.93	-179.80	-179.75	-179.74	-179.74
H18-C3-N4-C5	67.88	66.71	66.42	66.34	66.31
H19-C3-H18-N6	179.93	179.80	179.76	179.75	179.73
H20-C5-N6-C1	-173.83	-174.14	-174.26	-174.31	-174.34
H21-C5-H20-N2	180.00	180.00	180.00	180.00	180.00

TABLE IV.

Geometric Changes with respect to $\epsilon = 1$

Coordinate	$\epsilon = 5$	$\epsilon = 15$	$\epsilon = 30$	$\epsilon = 40$	Max Change
†C5-N4	.0030	.0040	.0042	.0043	.30%
†N6-C5	.0030	.0039	.0041	.0043	.30%
†N7-N6	-.0026	-.0034	-.0037	-.0037	-.27%
†N10-N4	-.0025	-.0033	-.0035	-.0037	-.27%
†N13-N2	-.0047	-.0066	-.0073	-.0075	-.55%
‡C3-N2-C1	-.32	-.33	-.32	-.32	-.29%
‡N4-C3-N2	-.49	-.61	-.64	-.64	-.59%
‡C5-N4-C3	-.29	-.38	-.40	-.41	-.36%
‡O8-N7-N6	.24	.32	.32	.35	.31%
‡O9-N7-O8	-.34	-.44	-.47	-.50	-.40%
‡N10-N4-C3	-.34	-.43	-.44	-.43	-.38%
‡O11-N10-N4	.24	.32	.32	.34	.30%
‡O12-N10-O11	-.34	-.44	-.46	-.49	-.39%
‡N13-N2-C1	1.62	2.18	2.36	2.41	2.08%
‡N4-C3-N2-C1	1.79	2.16	2.23	2.27	4.16%
‡C5-N4-C3-N2	-.88	-1.07	-1.11	-1.12	2.18%
‡N6-C5-N4-C3	.25	.36	.42	.42	.85%
‡N7-N6-C5-N4	-1.56	-2.00	-2.15	-2.17	-2.30%
‡N10-N4-C3-N2	-2.16	-2.68	-2.82	-2.79	-3.02%
‡N13-N2-C1-N6	-6.37	-8.62	-9.35	-9.55	-5.73%
‡O8-N7-N6-C5	1.09	1.45	1.55	1.48	6.42%
‡O9-N7-O8-N6	-.34	-.44	-.44	-.47	.28%
‡O12-N10-O11-N4	.33	.42	.42	.46	.27%
‡O14-N13-N2-C1	2.24	3.20	3.55	3.55	2.25%
‡O15-N13-O14-N2	.68	.83	.89	.88	-.51%
‡H16-C1-N2-C3	-2.26	-2.75	-2.86	-2.91	-4.67%
‡H18-C3-N4-C5	-1.17	-1.47	-1.55	-1.58	-2.32%
‡H20-C5-N6-C1	-.31	-.43	-.47	-.51	.29%

† Å

‡ degrees

TABLE V.

RDX Frequencies (cm^{-1}) vs. Dielectric Constant ϵ (Part A.)

ν	$\epsilon = 1$	$\epsilon = 5$	$\epsilon = 15$	$\epsilon = 30$	$\epsilon = 40$
1	36.6	39.4	40.1	40.0	40.2
2	62.7	56.5	53.1	51.8	51.5
3	66.4	68.7	69.2	69.5	69.4
4	73.5	73.5	73.4	73.5	73.3
5	96.6	98.7	99.7	100.1	100.2
6	119.7	125.7	127.4	128.1	127.8
7	235.0	238.1	238.8	239.1	239.1
8	248.3	236.5	231.3	229.5	229.0
9	327.8	331.5	332.3	332.6	332.6
10	364.9	370.5	372.3	372.9	373.0
11	417.7	419.5	420.1	420.1	420.0
12	451.3	461.1	463.7	464.5	464.5
13	456.3	458.9	459.2	459.4	459.1
14	501.9	508.9	510.6	511.3	511.2
15	538.0	545.4	547.3	547.9	547.9
16	644.8	648.3	649.5	650.0	650.1
17	669.7	666.2	665.0	664.7	664.5
18	689.7	687.6	686.5	686.3	686.1
19	740.5	736.0	734.3	733.9	733.8
20	754.1	751.5	750.3	750.0	749.9
21	861.6	858.7	857.2	856.7	856.6
22	890.4	892.6	892.9	893.0	893.0
23	899.1	897.1	895.9	895.5	895.4
24	917.8	918.4	918.3	918.3	918.3
25	957.4	954.6	953.5	953.2	953.2
26	978.9	975.8	974.4	974.0	973.9
27	995.9	991.9	990.0	989.5	989.3
28	1067.1	1058.9	1056.2	1055.5	1055.3
29	1072.1	1067.1	1065.2	1064.7	1064.5

TABLE VI.

RDX Frequencies (cm^{-1}) vs. Dielectric Constant ϵ (Part B.)

ν	$\epsilon = 1$	$\epsilon = 5$	$\epsilon = 15$	$\epsilon = 30$	$\epsilon = 40$
30	1100.6	1100.3	1100.0	1099.9	1099.9
31	1187.4	1183.1	1181.3	1181.0	1180.8
32	1190.7	1191.1	1191.3	1191.5	1191.6
33	1297.5	1290.2	1287.6	1287.0	1286.7
34	1385.0	1386.4	1387.2	1387.6	1387.7
35	1397.7	1400.2	1399.3	1399.1	1399.0
36	1414.8	1411.4	1411.1	1411.3	1411.3
37	1421.6	1418.8	1417.4	1417.1	1416.9
38	1492.5	1491.1	1490.2	1490.0	1489.9
39	1504.8	1503.3	1502.4	1502.3	1502.2
40	1520.1	1519.1	1518.4	1518.2	1518.3
41	1533.8	1528.4	1526.3	1525.8	1525.5
42	1534.2	1530.3	1529.2	1529.0	1528.9
43	1585.8	1583.0	1581.6	1581.3	1581.2
44	1593.2	1592.0	1591.1	1590.9	1590.9
45	1614.5	1610.4	1608.5	1608.0	1607.9
46	1637.3	1635.8	1634.8	1634.6	1634.6
47	1644.5	1644.9	1644.4	1644.3	1644.3
48	1667.7	1668.0	1667.6	1667.5	1667.5
49	1847.3	1840.2	1837.0	1836.1	1835.8
50	1868.5	1857.5	1853.8	1852.8	1852.5
51	1892.3	1879.8	1875.6	1874.6	1874.2
52	3239.9	3253.1	3256.1	3257.2	3257.6
53	3243.4	3256.1	3259.0	3260.1	3260.4
54	3301.8	3313.4	3315.4	3316.2	3316.4
55	3458.6	3460.9	3460.5	3460.4	3460.6
56	3464.3	3467.8	3467.5	3467.7	3467.8
57	3465.6	3469.0	3468.6	3468.8	3468.9

TABLE VII.

Frequency Changes (cm^{-1}) with respect to $\epsilon = 1$

ν	$\epsilon = 5$	$\epsilon = 15$	$\epsilon = 30$	$\epsilon = 40$	Max Change
1	2.8	3.5	3.4	3.6	10.08%
2	-6.2	-9.6	-10.8	-11.2	-17.87%
3	2.3	2.8	3.1	3.0	4.68%
5	2.1	3.1	3.5	3.6	3.75%
6	6.1	7.7	8.4	8.1	7.03%
7	3.1	3.9	4.1	4.1	1.77%
8	-11.8	-17.0	-18.8	-19.3	-7.78%
9	3.7	4.4	4.7	4.8	1.45%
10	5.6	7.4	8.0	8.1	2.22%
11	1.7	2.4	2.4	2.3	.60%
12	9.8	12.4	13.2	13.2	2.96%
13	2.6	2.9	3.0	2.8	.67%
14	7.0	8.7	9.3	9.2	1.86%
15	7.4	9.3	9.9	9.9	1.85%
16	3.5	4.7	5.2	5.3	.82%
17	-3.6	-4.8	-5.1	-5.2	-.78%
19	-4.5	-6.2	-6.6	-6.7	-.91%
20	-2.7	-3.8	-4.1	-4.2	-.56%
21	-2.8	-4.4	-4.9	-5.0	-.58%
27	-4.0	-5.9	-6.4	-6.6	-.66%
28	-8.1	-10.9	-11.5	-11.8	-1.11%
29	-5.1	-7.0	-7.4	-7.6	-.71%
31	-4.3	-6.1	-6.4	-6.6	-.56%
33	-7.3	-9.9	-10.5	-10.8	-.83%
49	-7.1	-10.3	-11.2	-11.6	-.63%
50	-11.0	-14.7	-15.7	-16.0	-.86%
51	-12.5	-16.7	-17.7	-18.1	-.96%

TABLE VIII.

IR Spectral Intensity (km/mol) vs. Dielectric Constant ϵ (Part A)

ν	$\epsilon = 1$	$\epsilon = 5$	$\epsilon = 15$	$\epsilon = 30$	$\epsilon = 40$
1	.03	.08	.11	.11	.11
2	4.01	6.33	6.78	6.90	6.91
3	2.08	1.06	1.00	.98	1.00
4	.02	.01	.00	.00	.00
5	.20	.33	.38	.39	.39
6	.08	.15	.18	.19	.19
7	10.13	13.80	15.00	15.35	15.45
8	.96	.99	.92	.89	.88
9	.10	.15	.18	.19	.19
10	2.08	2.73	3.02	3.13	3.15
11	.00	.00	.01	.01	.01
12	.20	.06	.04	.03	.03
13	11.30	14.57	15.57	16.01	16.02
14	12.54	17.69	19.42	19.77	19.95
15	5.64	6.30	6.48	6.55	6.60
16	16.66	22.27	23.79	24.19	24.32
17	15.58	23.89	27.23	28.31	28.59
18	45.94	68.21	76.11	78.49	79.18
19	10.33	12.25	12.60	12.67	12.70
20	8.77	10.68	11.10	11.20	11.22
21	3.43	10.06	14.01	15.47	15.89
22	14.26	17.21	17.88	18.04	18.09
23	4.09	13.66	18.85	20.57	20.96
24	84.47	111.36	118.82	120.98	121.63
25	70.29	70.75	69.02	68.24	67.97
26	3.91	10.69	13.68	14.62	14.93
27	25.31	29.84	30.98	31.29	31.25
28	158.15	225.81	247.26	253.39	254.85
29	145.13	184.42	195.91	198.87	199.95

TABLE IX.

IR Spectral Intensity (km/mol) vs. Dielectric Constant ϵ (Part B)

ν	$\epsilon = 1$	$\epsilon = 5$	$\epsilon = 15$	$\epsilon = 30$	$\epsilon = 40$
30	56.28	77.85	84.46	86.44	87.04
31	88.29	99.69	102.22	102.83	103.19
32	209.36	253.41	264.87	267.77	268.73
33	.75	.19	.08	.06	.05
34	37.32	44.20	45.92	46.35	46.46
35	12.51	16.72	24.25	26.85	27.68
36	42.97	53.89	51.41	50.33	49.98
37	.75	.73	.71	.72	.70
38	117.65	200.20	237.30	249.79	253.38
39	8.93	9.79	10.33	10.34	10.47
40	63.38	63.25	59.94	58.88	58.39
41	91.57	123.50	135.46	138.93	140.14
42	261.97	304.84	308.61	308.38	307.91
43	89.84	120.90	130.43	132.98	134.32
44	243.57	292.20	304.78	308.64	309.16
45	268.49	375.22	412.90	424.25	427.58
46	64.42	57.99	54.90	53.59	53.43
47	1.11	2.54	3.22	3.47	3.50
48	105.64	132.15	141.99	145.35	146.35
49	61.32	110.07	139.67	149.38	155.38
50	721.41	792.24	792.41	791.23	786.56
51	805.09	980.23	1029.88	1043.08	1047.44
52	2.29	1.61	1.40	1.35	1.33
53	43.39	35.83	32.97	32.08	31.82
54	18.34	11.80	10.00	9.51	9.37
55	13.71	16.64	17.49	17.73	17.79
56	14.71	16.37	16.81	16.91	16.94
57	7.92	10.08	10.84	11.09	11.15

TABLE X.

IR Spectral Intensity Changes (km/mol) with respect to $\epsilon = 1$

ν	$\epsilon = 5$	$\epsilon = 15$	$\epsilon = 30$	$\epsilon = 40$	Max Change
1	.05	.07	.08	.08	249.85%
2	2.32	2.77	2.89	2.90	72.44%
3	-1.02	-1.08	-1.09	-1.07	-52.66%
4	-.01	-.01	-.01	-.01	-80.66%
5	.14	.18	.20	.20	102.31%
6	.07	.10	.11	.11	142.35%
7	3.67	4.87	5.22	5.31	52.42%
9	.05	.08	.09	.10	100.00%
10	.66	.95	1.05	1.07	51.42%
11	.00	.00	.01	.01	152.17%
12	-.14	-.17	-.17	-.17	-85.29%
13	3.27	4.27	4.71	4.72	41.81%
14	5.15	6.88	7.23	7.41	59.43%
16	5.61	7.13	7.53	7.66	46.01%
17	8.31	11.64	12.72	13.01	83.46%
18	22.27	30.17	32.55	33.23	72.34%
21	6.62	10.58	12.04	12.45	362.58%
23	9.57	14.75	16.47	16.86	411.94%
24	26.89	34.35	36.51	37.16	43.99%
26	6.78	9.77	10.71	11.02	281.96%
28	67.67	89.11	95.25	96.70	61.15%
29	39.29	50.78	53.74	54.82	37.78%
30	21.57	28.18	30.16	30.76	54.65%
33	-.56	-.67	-.69	-.70	-93.22%
35	4.20	11.73	14.34	15.17	121.20%
38	82.55	119.65	132.14	135.73	115.37%
41	31.93	43.89	47.35	48.57	53.04%
43	31.05	40.59	43.14	44.47	49.50%
45	106.72	144.41	155.76	159.09	59.25%
47	1.43	2.11	2.36	2.39	216.98%
48	26.52	36.35	39.72	40.71	38.54%
49	48.75	78.35	88.06	94.05	153.38%
51	175.13	224.78	237.99	242.35	30.10%
52	-.68	-.89	-.94	-.96	-41.88%
54	-6.53	-8.34	-8.83	-8.96	-48.88%
57	2.16	2.92	3.17	3.23	40.81%

TABLE XI.

Raman Spectral Intensity ($\text{\AA}^4/\text{amu}$) vs. Dielectric Constant ϵ (Part A)

ν	$\epsilon = 1$	$\epsilon = 5$	$\epsilon = 15$	$\epsilon = 30$	$\epsilon = 40$
1	2.19	3.41	3.82	3.94	3.98
2	.33	.91	1.12	1.19	1.20
3	2.61	3.61	3.94	4.03	4.08
4	.77	1.05	1.12	1.14	1.14
5	.58	.99	1.17	1.22	1.24
6	1.28	1.81	1.98	2.04	2.05
7	1.28	2.18	2.48	2.56	2.59
8	.58	.72	.74	.74	.74
9	.02	.04	.05	.05	.05
10	1.50	2.59	2.96	3.08	3.10
11	.31	.25	.22	.21	.21
12	.71	1.36	1.62	1.70	1.72
13	3.38	4.90	5.31	5.39	5.43
14	1.34	2.08	2.37	2.48	2.51
15	3.65	5.45	6.05	6.22	6.26
16	2.67	3.55	3.71	3.73	3.74
17	1.40	2.08	2.34	2.42	2.44
18	2.05	3.46	4.00	4.16	4.20
19	.33	.39	.40	.40	.41
20	1.19	1.75	1.93	1.97	1.99
21	.96	1.55	1.78	1.86	1.88
22	.08	.12	.13	.13	.14
23	.32	.66	.80	.85	.86
24	4.93	7.07	7.67	7.84	7.84
25	5.98	9.31	10.36	10.65	10.75
26	3.67	5.40	5.93	6.09	6.12
27	7.89	13.14	15.08	15.69	15.85
28	2.11	3.13	3.42	3.51	3.52
29	.47	.61	.66	.68	.68

TABLE XII.

Raman Spectral Intensity ($\text{\AA}^4/\text{amu}$) vs. Dielectric Constant ϵ (Part B)

ν	$\epsilon = 1$	$\epsilon = 5$	$\epsilon = 15$	$\epsilon = 30$	$\epsilon = 40$
30	3.54	4.78	5.19	5.31	5.34
31	2.50	3.41	3.71	3.80	3.82
32	1.63	2.60	2.99	3.10	3.14
33	.24	.27	.27	.27	.27
34	.18	.16	.15	.15	.14
35	4.20	4.36	3.68	3.49	3.41
36	1.99	5.75	7.96	8.65	8.87
37	.12	.24	.29	.31	.32
38	5.33	7.17	8.04	8.34	8.43
39	.50	.80	.88	.87	.90
40	1.34	2.30	2.78	2.93	2.98
41	7.06	10.68	11.83	12.22	12.27
42	7.92	15.49	18.39	19.26	19.49
43	10.43	15.43	17.06	17.51	17.70
44	14.54	19.98	21.33	21.64	21.72
45	16.95	29.98	34.97	36.51	36.98
46	4.84	6.47	6.86	6.97	6.98
47	7.15	10.55	11.62	11.92	11.99
48	6.14	8.91	9.83	10.11	10.19
49	.06	.09	.09	.09	.09
50	.36	.37	.38	.39	.39
51	.53	.79	.92	.97	.98
52	11.20	14.40	15.42	15.74	15.79
53	114.90	163.53	178.88	183.35	184.45
54	95.74	130.12	141.44	144.83	145.69
55	22.36	38.16	43.67	45.44	45.82
56	13.77	19.34	21.17	21.73	21.93
57	38.09	58.37	65.19	67.00	67.55

TABLE XIII.

Raman Spectral Intensity Changes ($\text{\AA}^4/\text{amu}$) with respect to $\epsilon = 1$

ν	$\epsilon = 5$	$\epsilon = 15$	$\epsilon = 30$	$\epsilon = 40$	Max Change
1	1.22	1.63	1.75	1.78	81.39%
2	.58	.79	.86	.86	260.99%
5	.41	.59	.64	.66	114.98%
6	.53	.71	.77	.77	60.40%
7	.89	1.19	1.28	1.30	101.51%
9	.02	.02	.03	.03	116.22%
10	1.10	1.47	1.58	1.60	106.96%
12	.65	.91	.99	1.01	142.97%
13	1.52	1.93	2.01	2.05	60.83%
14	.74	1.02	1.14	1.16	86.56%
15	1.81	2.41	2.57	2.61	71.63%
17	.68	.94	1.03	1.05	74.97%
18	1.41	1.94	2.10	2.15	104.58%
20	.56	.73	.78	.79	66.50%
21	.59	.82	.90	.92	95.24%
22	.04	.05	.05	.05	61.81%
23	.33	.48	.52	.53	164.85%
25	3.33	4.38	4.67	4.77	79.80%
26	1.73	2.26	2.41	2.44	66.56%
27	5.25	7.19	7.79	7.95	100.80%
28	1.01	1.30	1.39	1.41	66.58%
32	.97	1.36	1.47	1.51	92.57%
36	3.75	5.96	6.65	6.88	345.03%
37	.12	.18	.19	.20	165.27%
39	.30	.38	.37	.40	80.53%
40	.97	1.44	1.59	1.64	123.93%
41	3.62	4.77	5.16	5.21	73.70%
42	7.57	10.47	11.34	11.57	146.12%
43	5.00	6.63	7.08	7.27	69.68%
45	13.03	18.02	19.56	20.03	118.15%
47	3.41	4.47	4.78	4.84	67.77%
48	2.77	3.69	3.97	4.05	65.94%
51	.27	.40	.44	.45	85.95%
53	48.63	63.98	68.45	69.55	60.53%
55	15.80	21.30	23.07	23.45	104.87%
57	20.28	27.10	28.91	29.46	77.35%

TABLE XIV.

Atomic Charges (esu) vs. Dielectric Constant ϵ

Atom	$\epsilon = 1$	$\epsilon = 5$	$\epsilon = 15$	$\epsilon = 30$	$\epsilon = 40$
C1	.0488	.0418	.0401	.0396	.0394
N2	-.5051	-.5168	-.5206	-.5218	-.5220
C3	.0489	.0418	.0400	.0396	.0396
N4	-.4832	-.4715	-.4679	-.4669	-.4667
C5	.0047	-.0032	-.0055	-.0063	-.0064
N6	-.4832	-.4715	-.4680	-.4669	-.4667
N7	.8514	.8473	.8460	.8456	.8455
O8	-.4637	-.4651	-.4656	-.4657	-.4659
O9	-.4783	-.4882	-.4911	-.4919	-.4920
N10	.8514	.8473	.8460	.8456	.8454
O11	-.4637	-.4651	-.4656	-.4657	-.4657
O12	-.4783	-.4882	-.4910	-.4918	-.4921
N13	.8599	.8659	.8681	.8688	.8689
O14	-.4818	-.4869	-.4890	-.4897	-.4899
O15	-.4818	-.4869	-.4890	-.4897	-.4899
H16	.2216	.2378	.2427	.2442	.2446
H17	.3188	.3171	.3168	.3167	.3167
H18	.2216	.2378	.2427	.2442	.2446
H19	.3188	.3171	.3168	.3167	.3166
H20	.3267	.3264	.3263	.3264	.3263
H21	.2466	.2630	.2678	.2692	.2695

TABLE XV.

Changes in Atomic Charges (esu) with respect to $\epsilon = 1$

Atom	$\epsilon = 5$	$\epsilon = 15$	$\epsilon = 30$	$\epsilon = 40$	Max Change
C1	-0.0070	-0.0087	-0.0092	-0.0094	-19.35%
N2	-0.0117	-0.0155	-0.0167	-0.0169	3.35%
C3	-0.0071	-0.0089	-0.0093	-0.0093	-19.17%
N4	.0117	.0153	.0163	.0165	-3.42%
C5	-0.0078	-0.0102	-0.0110	-0.0110	-236.26%
N6	.0116	.0151	.0162	.0164	-3.40%
N7	-0.0041	-0.0053	-0.0058	-0.0059	-.69%
O9	-0.0099	-0.0127	-0.0136	-0.0137	2.86%
N10	-0.0041	-0.0054	-0.0058	-0.0060	-.70%
O12	-0.0098	-0.0126	-0.0135	-0.0138	2.88%
N13	.0060	.0082	.0089	.0091	1.06%
O14	-0.0050	-0.0071	-0.0078	-0.0080	1.67%
O15	-0.0050	-0.0072	-0.0078	-0.0081	1.67%
H16	.0161	.0211	.0226	.0230	10.37%
H17	-0.0017	-0.0021	-0.0022	-0.0022	-.68%
H18	.0161	.0211	.0226	.0230	10.36%
H19	-0.0017	-0.0021	-0.0022	-0.0022	-.69%
H21	.0165	.0213	.0226	.0230	9.32%

TABLE XVI.

Dipole Moments (Debye) of RDX

ϵ	μ			Total	$\frac{\mu_x}{\mu_y}$
	x	y	z		
1	0.4621	0.0002	6.5815	6.5977	1.00
5	0.3477	-0.0002	7.6604	7.6682	1.16
10	0.3091	-0.0003	7.9009	7.9069	1.20
15	-0.2914	-0.0001	7.9905	7.9958	1.21
20	-0.2819	0.0008	8.0401	8.0450	1.22
25	-0.2792	-0.0001	8.0673	8.0721	1.22
30	-0.2745	-0.0003	8.0873	8.0920	1.23
35	0.2681	0.0091	8.1084	8.1128	1.23
40	0.2701	-0.0002	8.1148	8.1193	1.23

TABLE XVII.

Absolute Energy and Zero-Point Energy

ϵ	Absolute (hartrees)	Zero Point (kcal/mol)
1	-892.5070661	89.6016
5	-892.5116593	89.5780
10	-892.5126436	89.5421
15	-892.5130080	89.5364
20	-892.5131980	89.5331
25	-892.5133144	89.5312
30	-892.5133932	89.5302
35	-892.5134501	89.5271
40	-892.5134930	89.5250

TABLE XVIII.

Temperature-Corrected (323 K) Thermodynamic Functions (kcal/mole)

ϵ	ΔH	$T\Delta S$	ΔG
1	0.0000	0.0000	0.0000
5	-2.9385	0.0704	-2.8681
10	-3.5717	0.0658	-3.5059
15	-3.8057	0.0617	-3.7440
20	-3.9280	0.0582	-3.8699
25	-4.0029	0.0556	-3.9473
30	-4.0533	0.0546	-3.9987
35	-4.0911	0.0505	-4.0406
40	-4.1195	0.0481	-4.0714

TABLE XVII.

Absolute Energy and Zero-Point Energy

ϵ	Absolute (hartrees)	Zero Point (kcal/mol)
1	-892.5070661	89.6016
5	-892.5116593	89.5780
10	-892.5126436	89.5421
15	-892.5130080	89.5364
20	-892.5131980	89.5331
25	-892.5133144	89.5312
30	-892.5133932	89.5302
35	-892.5134501	89.5271
40	-892.5134930	89.5250

TABLE XVIII.

Temperature-Corrected (323 K) Thermodynamic Functions (kcal/mole)

ϵ	ΔH	$T\Delta S$	ΔG
1	0.0000	0.0000	0.0000
5	-2.9385	0.0704	-2.8681
10	-3.5717	0.0658	-3.5059
15	-3.8057	0.0617	-3.7440
20	-3.9280	0.0582	-3.8699
25	-4.0029	0.0556	-3.9473
30	-4.0533	0.0546	-3.9987
35	-4.0911	0.0505	-4.0406
40	-4.1195	0.0481	-4.0714

CHAPTER V

Conclusions

Hartree–Fock self-consistent–field methods[9,10,16] coupled with Onsager theory[7,8,11] have been used to study the changes in the molecular properties of RDX induced by solvents of varying dielectric constants. Changes in geometric parameters, harmonic vibrational frequencies, Gibbs free energy, infrared and Raman spectral intensities, atomic charge distributions, and dipole moments have been calculated.

The results indicate that most of the changes which occur approach limiting values at or before $\epsilon = 20$. Only the infrared and Raman intensities and components of the dipole moment of RDX change significantly with increasing dielectric constant of the solvent. All other molecular properties have minimal change as ϵ increases.

The level of theory used here is not flexible enough to give a quantitative representation of the changes with respect to increasing dielectric constant. The directions of the trends, however, are probably correct. Improvements, left for future work, would be first to use a better basis set such as the triple zeta plus one diffuse valence function. This would allow the electronic cloud to respond more completely to the applied external field. The next step would be to include correlation effects (such as second-order Møller-Plesset Perturbation theory) and density function theory using a hybrid functional like that Becke–3LYP. It is expected that with a more flexible basis set and correlation treatment that one would see a larger charge rearrangement in the molecule upon the application of a field.

The large changes in intensity for the infrared spectra as a function of increasing ϵ suggest that IR spectroscopy may be an effective tool for exploring the

microstructure around the RDX in a solvent. Comparisons of experimental and theoretical spectra could provide a guide for the number of modifiers surrounding the molecule in solution, as well as the nature of the interactions. For example, if the solvent molecules are complexed to RDX in solution, the infrared spectra should change significantly; however, if the RDX molecule is not bound or complexed in solution, then the trend in the changes in the spectral intensities should be similar to those predicted in this study.

Apart from changes in the charge distribution due to changing ϵ , the partial charges calculated with $\epsilon = 1$ (no field) give a good indication as to where one would expect to see hydrogen-bonding type arrangements between a polar modifier and the RDX modifier if such bonding occurs. These calculations confirm that the oxygens have a strong negative charge, which would make them good electron donors in a hydrogen-bonding situation.

The Gibbs free energy of solvation is negative for all $\epsilon > 1$. This negative free energy indicates that the RDX molecules attain a lower energy state, and are stabilized by the polar solvents. These calculations also show that the Gibbs free energy quickly reaches a plateau with increasing ϵ . Even though these calculations do not predict the solvent that provides the maximum stability of the molecule, it appears that there is a value of the dielectric constant beyond which modest to no additional stability is achieved.

BIBLIOGRAPHY

1. G. Mourou and A.H. Zewail, *Ultrafast Phenomena VIII*, Springer, New York, 1994.
2. P.J. Rossky and J.D. Simon, *Nature* **370**, 263 (1994) and references therein.
3. J. Tomasi, R. Bonaccorsi, F.J. del Olivares, *J. Mol. Struct.(THEOCHEM)* **234**, 407, (1991).
4. M.M. Karelson and M.C. Zerner, *J. Phys. Chem.* **96**, 6949 (1992).
5. C.J. Cramer and D.G. Truhlar, *Journal of Computer-Aided Molecular Design* **6**, 629 (1992) and references therein.
6. J.B. Morris, M.A. Schroeder, R.A. Pesce-Rodrigues, K.L. McNesby and R.A. Fifer, ARL-TR
7. L. Onsager, *J. Am. Chem. Soc.* **58**, 1486 (1938).
8. E. S. Amis, *Kinetics Of Chemical Change In Solution*, The MacMillan Company, New York, 1949.
9. I. N. Levine, *Quantum Chemistry*, Allyn and Bacon, Boston, 1983.
10. D. A. McQuarrie, *Quantum Chemistry*, University Science Books, California, 1983.
11. J. B. Foresman, and Æ. Frisch *Exploring Chemistry with Electronic Structure Methods: A Guide to Using Gaussian*, Gaussian Inc., Pittsburgh,
12. M. J. Frisch, G. W. Trucks, H. B. Schlegel, P. M. W. Gill, B. G. Johnson, M. W. Wong, J. B. Foresman, M. A. Robb, M. Head-Gordon, E. S. Replogle, R. Gomperts, J. L. Andres, K. Raghavachari, J. S. Binkley, C. Gonzalez, R. L. Martin, D. J. Fox, D. J. Defrees, J. Baker, J. J. P. Stewart, and J. A. Pople, *Gaussian 92/DFT, Revision G.1*, Gaussian, Inc., Pittsburgh PA, 1993.
13. C.S. Choi and E. Prince, *Acta Crystallogr. Sect B* **28**, 2875 (1972).
14. W.J. Hehre, R. Ditchfield, and J.A. Pople, *J. Chem. Phys.* **56**, 2257 (1972).
15. P.C. Hariharan and J.A. Pople, *Theor. Chim. Acta.* **28**, 213 (1973).
16. W.J. Hehre, L. Radom, P.v.R. Schleyer, and J. A. Pople *Ab Initio Molecular Orbital Theory* John Wiley & Sons, New York, 1986.
17. M.S. Gordon, *Chem. Phys. Lett.* **76**, 163 (1980).
18. M.W. Wong, K.B. Wiberg, and M.J. Frisch, *J. Chem. Phys.* **95**, 8991 (1991).

19. D. A. McQuarrie, *Statistical Mechanics*, HarperCollinsPublishers Inc., New York, 1976.
20. M.W. Wong, M.J. Frisch, and K.B. Wiberg, *J. Am. Chem. Soc.* **113**, 4776 (1991).
21. M.B. King and T.R. Bott, *Extraction Of Natural Products Using Near-Critical Solvents*, Blackie Academic & Professional, Glasgow, 1993.
22. M. Mchugh and V. Krukonis, *Supercritical Fluid Extraction. Principles and Practice*, Butterworths, Boston, 1986.

VITA

PAUL J. ZAHNER

Candidate for the Degree of

Master of Science

Thesis: SOLVATION OF RDX AS A FUNCTION OF THE DIELECTRIC
CONSTANT OF THE SOLVENT

Major Field: Chemistry

Biographical:

Personal Data: Born Tulsa, Oklahoma September 15, 1969, the son of Richard Patrick and Vera Lavern Zahner.

Education: Received Bachelor of Science Degree in Chemistry from Kansas Newman College, Wichita, KS 1992; Completed requirements for the Master of science Degree at Oklahoma State University, Stillwater Oklahoma July 1995

Professional Experience: Treasurer, Phi Lambda Upsilon 1993 – 1994; Teaching Assistant, Department of Chemistry, Oklahoma State University, January, 1994 – December, 1994; Research Assistant, Department of Chemistry, Oklahoma State University, May, 1993 – Dec, 1993 and January, 1995 – May 1995.